CHARGE EXCHANGE OF STOPPED π^- IN DEUTERIUM

by

RANDY NEIL MACDONALD

B.Sc., University of Alberta, Edmonton, Alberta, Canada

M.Sc., McMaster University, Hamilton, Ontario, Canada

A THESIS SUBMITTED IN PARTIAL FULFILMENT OF

THE REQUIREMENTS FOR THE DEGREE OF

DOCTOR OF PHILOSOPHY

IN THE FACULTY OF GRADUATE STUDIES

in the

Department of Physics

We accept this thesis as conforming to the

required standard

THE UNIVERSITY OF BRITISH COLUMBIA

August, 1977

In presenting this thesis in partial fulfilment of the requirements for an advanced degree at the University of British Columbia, I agree that the Library shall make it freely available for reference and study. I further agree that permission for extensive copying of this thesis for scholarly purposes may be granted by the Head of my Department or by his representatives. It is understood that copying or publication of this thesis for financial gain shall not be allowed without my written permission.

Department of Physics

The University of British Columbia
2075 Wesbrook Place
Vancouver, Canada
V6T 1W5

Date August 3,1977

ABSTRACT

By using a pair of large NaI spectrometers in a coincidence configuration we have observed the charge exchange of stopped π^- in deuterium

$$\pi^- + d \rightarrow 2n + \pi^0.$$

We have measured the branching ratio of this reaction

$$R = \frac{\omega(\pi^- d \rightarrow \pi^0 nn)}{\omega(\pi^- d \rightarrow \text{all})}$$

and find

$$R = (1.45 \pm 0.19) \times 10^{-4}.$$

This measurement is the first observation of pion charge exchange at rest in deuterium and represents an increase in sensitivity of a factor of 40 over previous measurements. The measured value of R agrees well with the recent theoretical result of Beder($1.39 \times 10^{-4} \leq R \leq 1.59 \times 10^{-4}$).

TABLE OF CONTENTS

LIST OF TABLES

LIST OF FIGURES

ACKNOWLEDGEMENTS

Like most experiments in this field this one was performed by a group of experimenters and I am grateful to each of them for the part he played. Included in this group were D.Berghofer, Dr. M.D. Hasinoff, Dr. D.F. Measday, Dr. M. Salomon, Dr. J. Spuller, T. Suzuki, Dr. J.M. Poutissou, Dr. R. Poutissou, Dr. P. Depommier, and Dr. J.K.P. Lee.

I appreciate the efforts made by my supervisor, Dr. M.D. Hasinoff, and Dr. D.F. Measday who have read this work in its draft form and made many useful suggestions. I am grateful for many useful discussions with Dr. D.S. Beder. In particular the work presented in Chapter IV and Appendix II has been derived from his notes. I am also grateful to Dr. A.W. Thomas for his assistance with the calculations presented in Appendix III. I thank D. Garner for his invaluable help with the μSR groups computing system. Finally I thank my wife Hilary for her part in typing the manuscript. I dedicate this work to my parents and Mr. J. Stanton.

CHAPTER I

INTRODUCTION

When negative pions interact at rest in deuterium three processes are energetically allowed.

1.	$\pi^- + d \rightarrow 2n$	absorption
2.	$\pi^- + d \rightarrow 2n + \gamma$	radiative capture
3.	$\pi^- + d \rightarrow 2n + \pi^o$	charge exchange.

Of these only the first two have been previously observed (PA51, CH54, KU59, RY63, KL64). Although searches had been made for the charge exchange reaction in deuterium (PA51, CH55) it had not been observed. In fact, the charge exchange reaction for pions at rest had only been observed in hydrogen (PA51, C061) and helium-3 (ZA65, TR74).

It is common to define the ratios

$$S = \frac{\omega(\pi^- d \rightarrow 2n)}{\omega(\pi^- d \rightarrow 2n\gamma)}$$

and

$$K = \frac{\omega(\pi^- d \rightarrow 2n\pi^o)}{\omega(\pi^- d \rightarrow 2n\gamma)}$$

or

$$R = \frac{\omega(\pi^- d \rightarrow 2n\pi^o)}{\omega(\pi^- d \rightarrow \text{all})}$$

where ω is the rate for the specified reaction. The previous experimental results are summarized in table I.1. It is interesting to note that those authors who have used liquid or gas targets have all measured a negative (although consistent with zero) branching ratio.

The failure to observe the charge exchange reaction in deuterium is a result of the identical parity of the π^- and π^0 (PA51, CH55, TA51, BR51). In hydrogen the absorption process ($\pi^- p \rightarrow n$) is forbidden by momentum-energy conservation and the allowed reactions are:

4. $\pi^- + p \rightarrow n + \gamma$ radiative capture,
5. $\pi^- + p \rightarrow n + \pi^0$ charge exchange.

In helium-3 the corresponding processes are:

6. $\pi^- + {}^3He \rightarrow {}^3H + \gamma$ radiative capture,
7. $\pi^- + {}^3He \rightarrow {}^3H + \pi^0$ charge exchange,

and the breakup reactions:

8. $\pi^- + {}^3He \rightarrow n + d$,
9. $\pi^- + {}^3He \rightarrow p + n + n$,
10. $\pi^- + {}^3He \rightarrow \gamma + n + d$,
11. $\pi^- + {}^3He \rightarrow \gamma + p + n + n$.

In all cases the π^- capture proceeds primarily from an s state (LE62). In the case of hydrogen and helium-3 the nuclear spin and parity is $\frac{1}{2}^+$. In the case of deuterium it is 1^+. For pseudoscalar pions we then have a total initial spin and parity $\frac{1}{2}^-$ in the case of hydrogen and helium-3.

TABLE I.1

EXPERIMENTER	VALUE OF S	VALUE OF R	VALUE OF K	METHOD OF OBSERVATION
Panofsky, Aamodt and Hadley (PA51)	2.36 ± 0.5	-0.007 ± 0.020	- 0.025 ± 0.072	Compare γ-ray yields from π^-d and π^-p reactions; gas target; pair spectrometer.
Chinowsky and Steinberger (CH54, (CH55)	1.5 ± 0.8	-8.3×10^{-4} $\pm 10.5 \times 10^{-4}$	-0.0034 ± 0.0043	S: Compare γ-ray single and neutron coincidence yields from π^-d reactions; K: Compare γ-ray singles and γ-ray coincidence yields from π^-d reactions; liquid target; liquid scintillator for neutrons; lead converter-plastic scintillator telescope for γ-rays.
Kuehner, Merrison and Tornabene (KU59)	2.39 ± 0.36			Compare γ-ray yields from π^-d and π^-p reactions; liquid target; pair spectrometer.
Ryan (RY63)	3.16 ± 0.10			Compare γ-ray yields from π^-d and π^-p reactions; liquid target; pair spectrometer.
Kloeppel (KL64)	2.89 : 0.09	-5.7×10^{-4} $\pm 6.7 \times 10^{-4}$	-2.3×10^{-3} $\pm 2.7 \times 10^{-3}$	γ-ray (internal conversion) yields from π^-d reactions in a bubble chamber.
Petrukin and Prokoshkin (PE64)		$<10^{-3}$	$<<4 \times 10^{-3}$	Coincidence γ-ray yields of LiDi lead glass detectors.

With no spin-flip the neutral pion will be emitted in an s state. In the case of deuterium however the initial state is 1^-. In the final state the two neutrons, being identical fermions, must have an anti-symmetric wave function. The only possibilities allowed are a singlet s wave (^1s) and a triplet p wave (^3p). In the case of a ^1s di-neutron wave function the neutral pion must be emitted in a p state to conserve angular momentum. This results in a final state with positive parity and hence it is forbidden. In the case of a ^3p di-neutron wave function the neutral pion must also be emitted in a p state relative to the di-neutron in order to conserve parity. Since the reaction is only slightly exothermic (Q = 1.10 MeV) the reaction rate is greatly retarded. Of course, from an historical perspective the above argument has been reversed and in fact it was the non-observation of a significant charge exchange rate in deuterium which led to the conclusion that the π^- and π^o must both be pseudoscalar particles (CH54, CH55).

For scalar mesons the absorption reaction (1) is forbidden for a π^- in an s-wave atomic state but could occur for capture from a p-wave atomic state. Brueckner et al (BR51) have used a detailed balance argument for the reaction $p + p \rightarrow d + \pi^+$ to determine the ratio 'S' for scalar pions absorbed from an atomic p-state and found a value which is a factor of 30 too small to account for the experimental value determined by Panofsky et al (PA51). On the other hand the calculated 'S' ratio for pseudoscalar pions, which can be captured from an s-wave atomic state, was found to be compatible with the experimental value.

Tamor (TA51) has calculated the rates for the three deuterium reactions (1,2,3) using all reasonable combinations of meson spins, parities and coupling theories. In the calculation mesons of both

positive and negative parity were considered. Negative mesons of spin 0 and 1 were considered; however the neutral meson was known to decay into 2 γ-rays and hence only spin zero neutral mesons had to be considered.

In the case of scalar π^- the absorption reaction is prohibited from the s-state and Tamor puts an upper limit of 4% on the number of mesons absorbed from atomic orbitals with higher angular momentum in essential agreement with Brueckner et al. If the π^- was a vector meson Tamor predicts a ratio S=55, again in distinct conflict with Panofsky's data, $S = 2.36 \pm 0.5$. The calculated ratios for both pseudoscalar and pseudovector mesons were compatible with the experimental value of S. For a pseudovector π^- he finds a negligible value of 'K' for either parity of π^0 and so nothing can be inferred from Panofsky's data. For a pseudoscalar π^- the calculated value of 'K' is negligible in the case of pseudoscalar π^0 but $K \simeq 0.1$ for scalar π^0. Thus the experimental data of Panofsky, and later data of Chinowsky et al (CH55) indicate that if the π^- is a pseudoscalar particle then the π^0 must also be a pseudoscalar particle.

We have now observed the charge exchange reaction in deuterium and have measured the ratios K and R to be

$$K = (5.71 \pm 0.82) \times 10^{-4}$$

$$R = (1.45 \pm 0.19) \times 10^{-4}$$

This is in agreement with a recent theoretical result of Beder (MA77)

$$1.39 \times 10^{-4} \leq R \leq 1.59 \times 10^{-4} .$$

The present work is a detailed description of the experimental work and the data analysis which derives these ratios. The experiment is described in Chapter II and the details of the data analysis are reported in Chapter III. Chapter IV includes a brief discussion of the theoretical values as well as the relationships of these values with other low energy pion data. The details of some calculations have been placed in appendices to avoid interrupting the flow of ideas. Appendix IV is a discussion of possible explanations for the anomolously low hydrogen contamination which was observed in the liquid deuterium target. Future experimental studies of the effects described in this appendix have been planned (ME77).

CHAPTER II

THE EXPERIMENT

1. Kinematic Considerations

The experimental method employs a coincidence technique to observe the 2γ decay of the neutral pion. The coincidence technique has two principle advantages over a singles technique. First, the dominant γ-ray singles background from the radiative capture process which overwhelms any small charge exchange component is eliminated and second, the coincidence geometry greatly favors the detection of the deuteron charge exchange π^0 (0.0 MeV$\leq T_{\pi^0}(d) \leq 1.1$ MeV) over the hydrogen charge exchange π^0 ($T_{\pi^0}(p) = 2.9$ MeV). To understand these advantages it is useful to first consider the γ-ray spectra which one would observe from the interaction of stopped π^- in hydrogen. As in the case of deuterium the γ-radiation arises from the radiative capture of the pions and also from the decay of the neutral pions formed in the charge exchange process. The radiative capture γ-ray is mono-energetic at 129.4 MeV. The neutral pion from the charge exchange reaction is likewise mono-energetic with $T_{\pi^0}(P) = 2.90$ MeV. Since the reactions take place at rest there is no preferred direction and the distributions of these γ-rays and pions will be isotropic. If one now observes the γ-decay of the π^0 in the lab frame, one sees a γ-ray with an energy which has been Doppler shifted by an amount which is determined by the π^0 momentum in the lab frame. In Appendix I.1 it is shown that

$$E_\gamma' = \frac{1}{2} \frac{m_\pi^2}{E_\pi - P_\pi \cos\Theta} \qquad \text{(II.1.1)}$$

where Θ is the angle between the observed γ-ray and the pion momentum (figure II.1.1). Thus we see a continuous distribution of γ-rays between the energy limits E_L and E_H

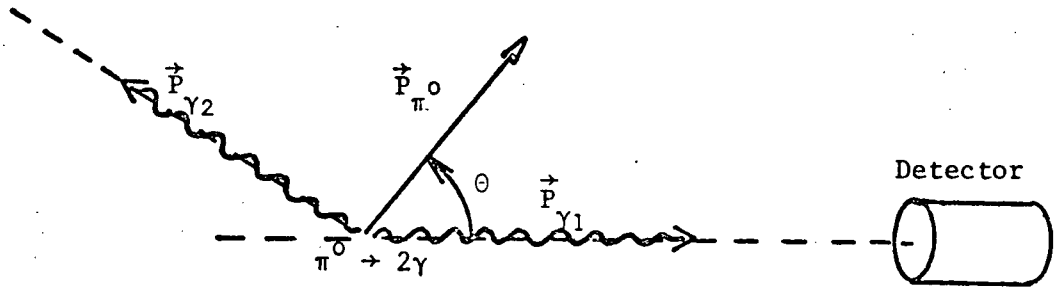

Figure II.1.1 π^o decay in the laboratory rest frame

determined by $\Theta = 0$ and $\Theta = \pi$; i.e.

$$E_{L,H} = \frac{1}{2} \frac{m_\pi^2}{E_\pi \pm P_\pi}$$

or

$$E_{H,L} = \frac{E_\pi \pm P_\pi}{2} \qquad \text{(II.1.2)}$$

In the case of hydrogen $E_L = 54.9$ MeV and $E_H = 83.0$ MeV. Further, as is shown in Appendix I.2, for an isotropically distributed mono-chromatic π^o the observed γ-ray spectrum is the box spectrum

$$\frac{dn_\gamma}{dE_\gamma} = \begin{cases} 0 & \text{for } E_\gamma < E_L \\ K & \text{for } E_L \leq E \leq E_H \\ 0 & \text{for } E > E_H \end{cases} .$$

These features can be seen in the measured γ-ray spectrum from stopped π^- in hydrogen (figure II.1.2). The deviations from a perfect rectangle and delta function are consistent with the finite resolution function of the spectrometer.

In the case of stopped π^- in deuterium the situation is complicated by the 3-body final state ($\pi^o nn$ and γnn). The γ-ray from the radiative capture channel is no longer mono-energetic but is spread over a range of energies from 0 MeV to 131.5 MeV. Although the γ-ray spectrum is more sharply peaked at high energies (due to the attractive low energy s-wave neutron-neutron interaction) than a simple phase-space calculation would predict there is still sufficient contribution in the medium energy range (∿70 MeV) to obliterate the details of the γ-ray spectrum from the π^o decay (figure II.1.3). Furthermore, the singles γ-ray decay spectrum of the deuterium π^o will be superimposed on the box spectrum created by the charge exchange in the hydrogen contamination (nominally 0.3%) of the deuterium target. Thus the separation of the small deuterium π^o γ-ray spectrum from the radiative capture background and hydrogen contamination would be a formidable problem. With hindsight it is possible to say that of the γ-ray spectrum measured in the 55 MeV to 83 MeV region only 3% is from charge exchange in deuterium.

Fortunately both of these backgrounds can be eliminated with a coincidence arrangement. That the radiative capture γ-rays are eliminated with a coincidence technique is obvious. That the deuterium

Figure II.1.2
The Gamma Ray Spectrum of Stopped Pions in Hydrogen

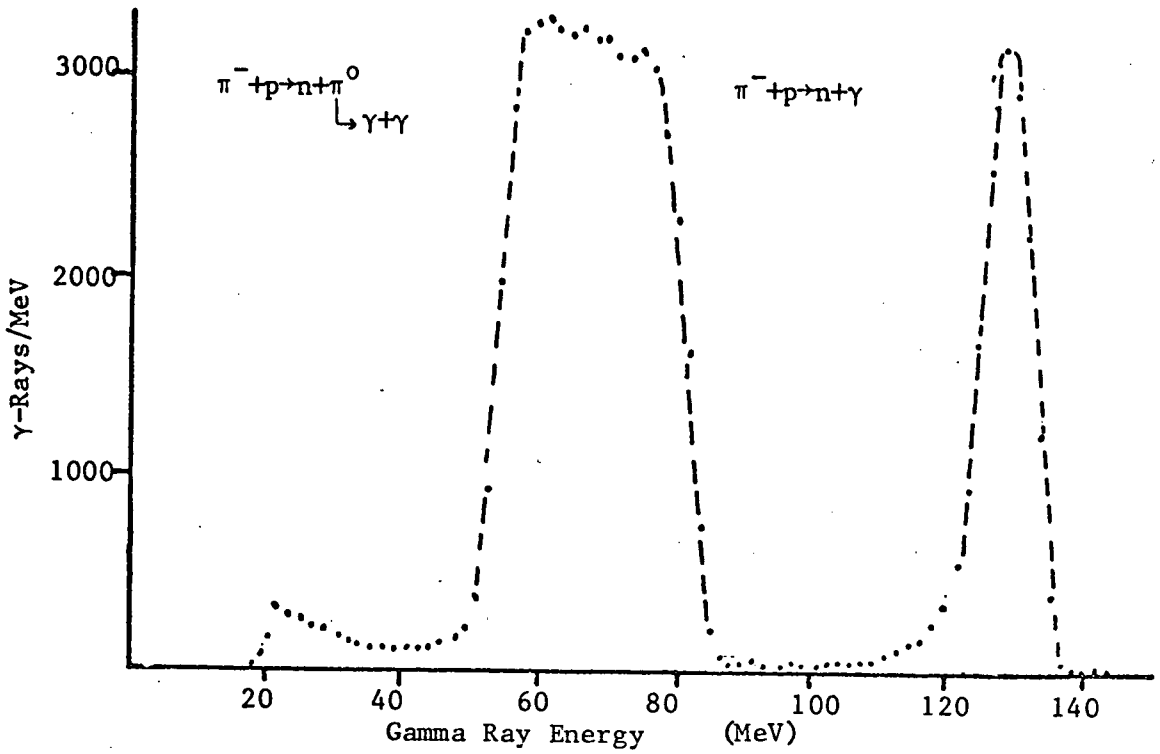

Figure II.1.3
Theoretical Gamma Ray Spectrum of Stopped Pions in Deuterium

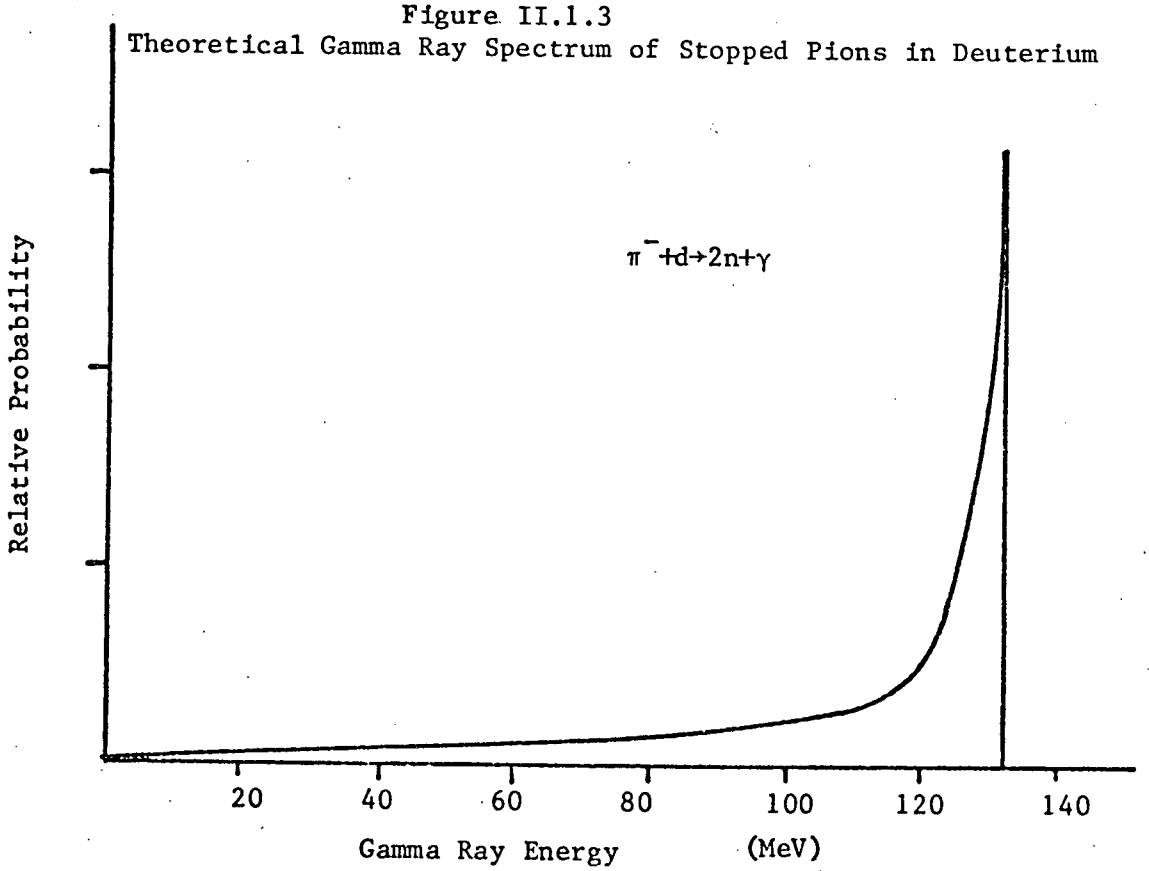

π^o decays may be separated from the hydrogen π^o decays is a fortunate consequence of the difference in Q-values for the two reactions and the good energy resolution of the NaI spectrometers.

If one knows the energy of the π^o before it decays and defines both the direction and energy of one of the decay γ-rays then the direction of the π^o momentum and the direction of the second γ-ray are determined up to an angle about the direction of the first γ-ray. (figure II.1.4) The angle Θ between the π^o and the first γ-ray is determined by (II.1.1) and using the conservation laws it can be shown (Appendix I.3) that the angle ϕ between the two γ-ray directions is given by the equation:

$$\cos\phi = \frac{E_\gamma^2 + (E_\pi - E_\gamma)^2 - P_\pi^2}{2E_\gamma(E_\pi - E_\gamma)} \quad . \qquad \text{(II.1.3)}$$

The second γ-ray must lie on the surface of a cone of half-angle ϕ generated by a rotation about the axis of the first γ-ray. It is clear

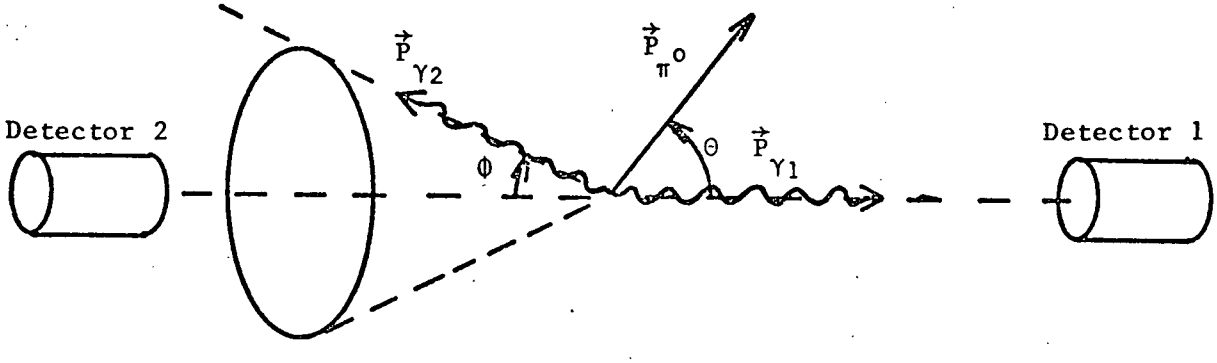

Figure II.1.4 The second γ-ray cone

that for detectors which subtend small solid angles there will only be a coincidence if $\phi \simeq 0$ or $\cos\phi \simeq 1$. From (II.1.3) we find that this requirement means

$$E_\gamma \simeq \frac{E_\pi \pm P_\pi}{2} \quad .$$

We recall (from (II.1.2)) that these are the maximum and minimum limits of the rectangular γ-ray spectrum. That is they correspond to the cases where the π^o is travelling in the forward or backward directions along the axis of the detectors. Hence, with small detectors and a small source one would expect to see only γ-rays at energies 54.9 MeV and 83.0 MeV from the hydrogen decays ($T_{\pi o}(p) = 2.90$ MeV).

Since the deuterium π^o's have a continuous spectrum due to the 3 body final state we would also expect the coincident γ-ray spectrum to be continuous with maximum limit 59.4 MeV and 76.7 MeV ($T_{\pi o}(d)_{max} = 1.1$ MeV). Thus the γ-rays from the hydrogen π^o decays will be separated in energy from the γ-rays which result from the deuterium π^o decays. Of course in any experiment it is necessary to have sources and detectors of finite size and the actual spectra obtained in each case must be determined by an integration over the detector surfaces and the target volume. This has the effect of allowing the hydrogen coincidence peaks to encroach somewhat on the deuterium coincidence spectrum. Detailed calculations of the coincident lineshapes and efficiencies have been performed for hydrogen and deuterium and are presented in chapter III of this work. The lineshapes shown in figure II.1.5 are the results for the geometry used in the present experiment and demonstrate the energy separation of the deuterium and hydrogen events. It is significant to note that the

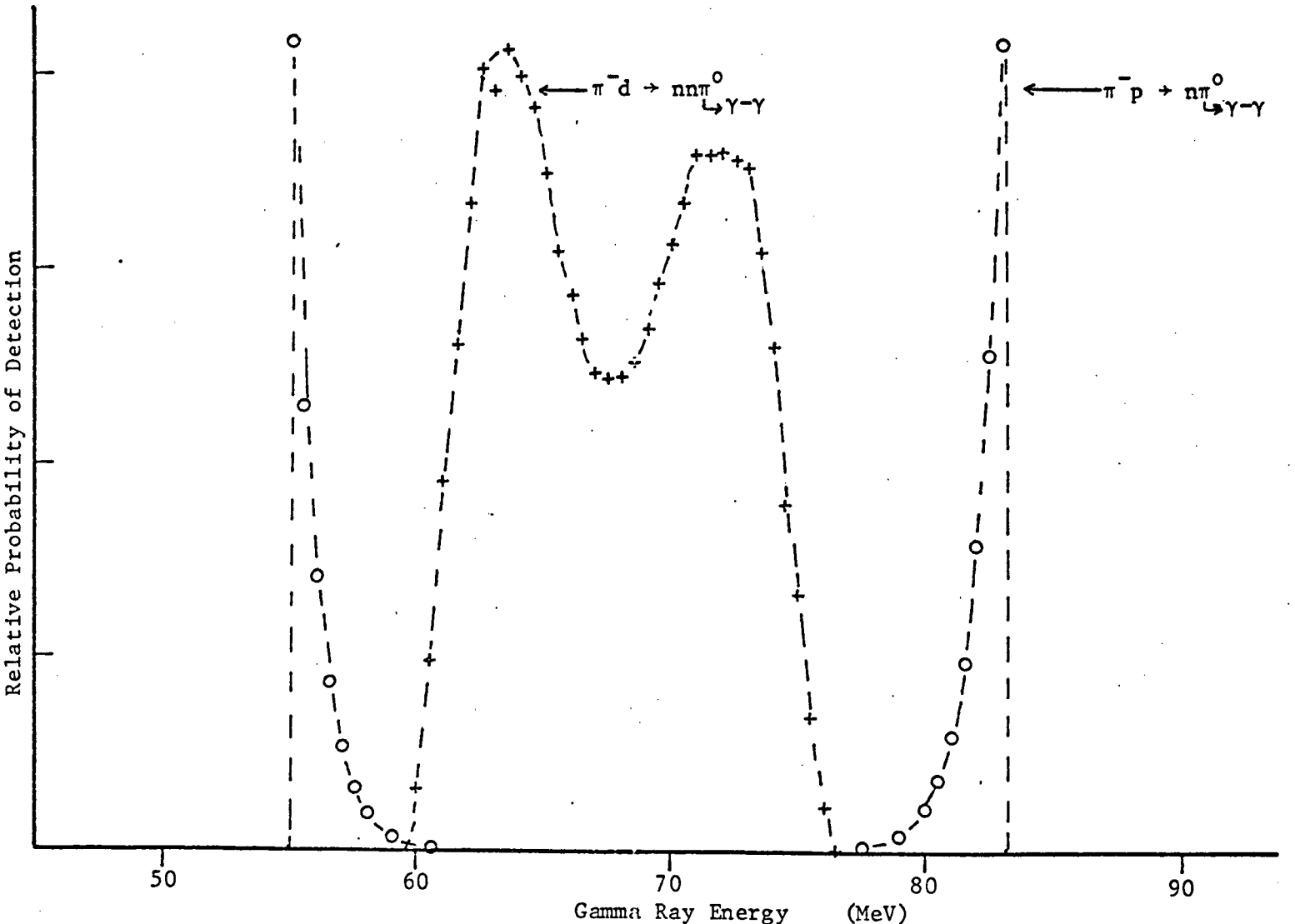

Figure II.1.5 Coincidence Lineshapes for Pion Charge Exchange

net coincidence detection efficiency for deuterium π^0 decays is 6.7 times larger than the corresponding efficiency for hydrogen π^0 decays.

2. The Spectrometers

The experiment was made feasible by the availability of two large sodium iodide spectrometers, TINA and MINA. TINA is a cylindrical block of NaI 45.7 cm. in diameter and 50.8 cm. in length. It is viewed by seven matched 12 cm. photomultiplier tubes (RCA 4522). MINA is a cylinder 35 cm. in diameter and 35 cm. long and is also viewed by four matched 12 cm. photomultiplier tubes (RCA 4522). The sodium iodide crystals are essentially 100% efficient and have sufficient resolving power to separate the coincident gamma rays originating from deuterium from those originating from hydrogen. Furthermore, the timing resolution of 2.0 nsec (FWHM) obtained with constant fraction discriminators makes it possible to separate the γ-rays from the large neutron background produced by the absorbtion and radiative capture channels. (The flight path of about 1 m. gives 6 nsec time separation between the γ-rays and the high energy neutrons). Figure II.2.1 shows the time spectrum of TINA and MINA and the separation of the γ-rays and neutrons. Figure II.2.2 shows the energy response of TINA and MINA to beams of high energy electrons. On the basis of an inverse square root relationship with energy one would anticipate an energy resolution of about 6.4% in TINA and 7.9% in MINA in the 55 MeV - 83 MeV range. In fact the resolution obtained in this range in the present experiment was about 10% in TINA and considerably larger than 10% in MINA. The increase in width in TINA may be attributed to the use of a large collimator (25 cm. diameter) and the problems of gain and zero instabilities encountered over a comparatively long period of time. The large width in MINA was found to be a result of insufficient voltages on the primary dynode stages of the photomultiplier tubes. The resolution in TINA was still

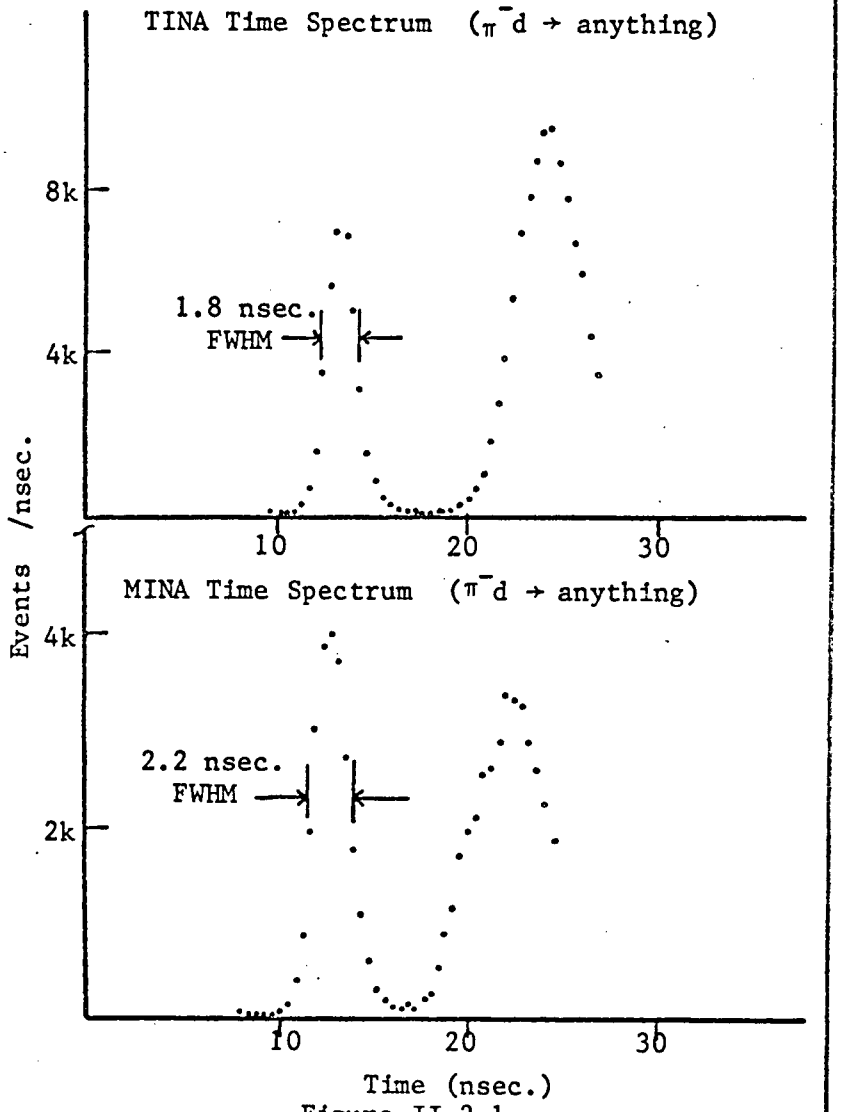

Figure II.2.1

Time Response of the NaI Spectrometers.

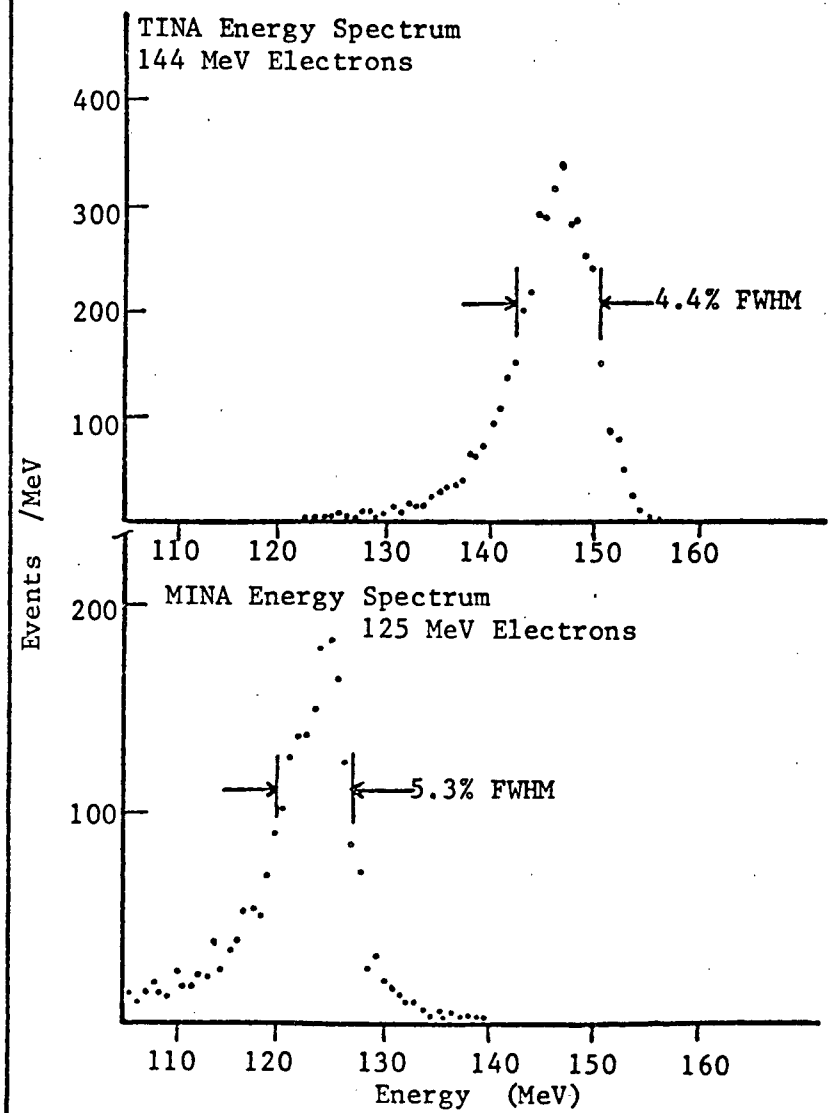

Figure II.2.2

High Energy Response of the NaI Spectrometers.

sufficient to separate the γ-rays from the deuterium and hydrogen charge exchange. The resolution in MINA was not sufficient in this respect. However MINA was used to provide a test of the total energy, $E_{TINA} + E_{MINA} = M + T$, and to form a two dimensional histogram of the coincidence events ($N_c(E_{TINA}, E_{MINA})$).

3. The Experimental Arrangement

Figure II.3.1 shows the configuration of our apparatus in the TRIUMF M-9 area. The pion beam was produced by a 1 μA beam of 500 MeV protons which strikes a 10 cm. beryllium target. The M-9 beam line was tuned for 51 MeV negative pions (momentum - 130 MeV/c). The beam contamination under these conditions was measured by time of flight and the beam was found to consist of 76% pions, 18% electrons and 6% muons (Figure II.3.2). The incident beam is defined by the plastic scintillators labelled C1 and C2 and degraded in a 2.9 cm. sheet of aluminum.

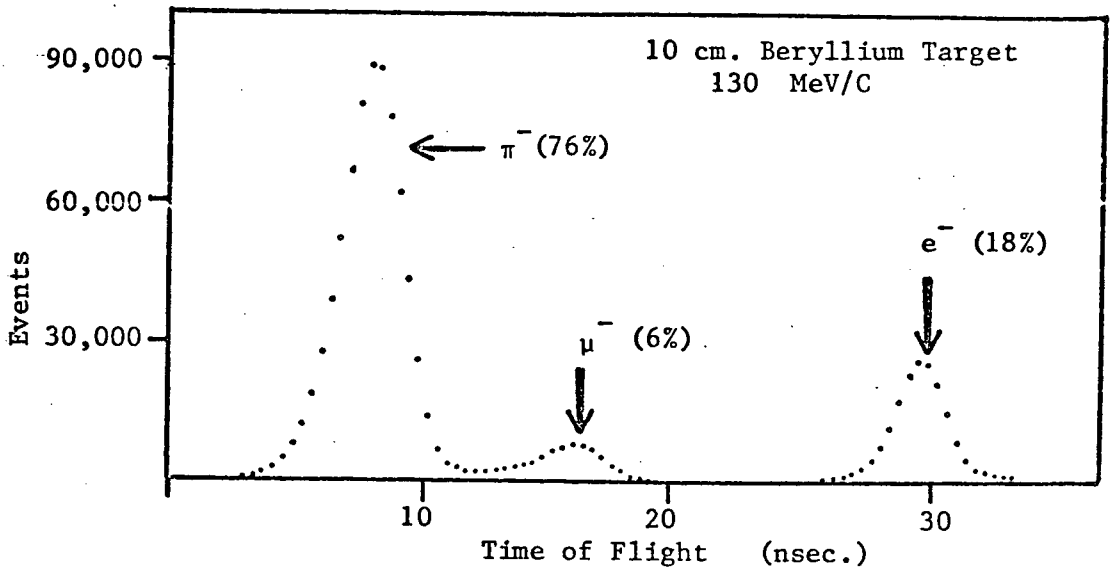

Figure II.3.2 The beam constitution

The target flask was a cylinder 15.5 ± 0.5 cm. long and 11.1 cm. in diameter giving a volume of 1.7 liters. The walls were 0.036 cm. mylar and the entrance window was 0.024 cm. mylar. The flask was wrapped in 10 layers of 6.4×10^{-4}cm. aluminized mylar to reduce the heat load. The deuterium was made by electrolyzing deuterium oxide which had a

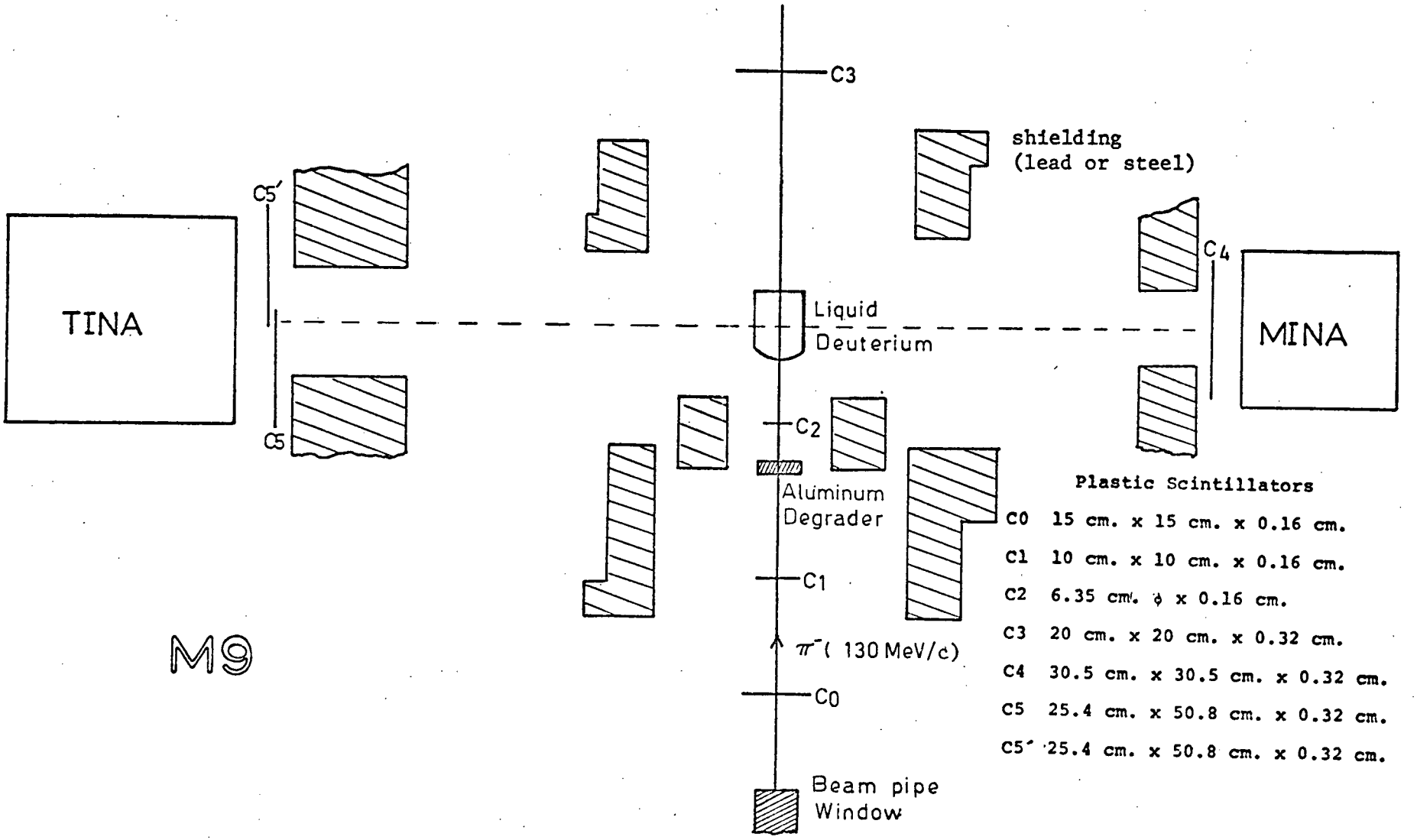

Figure II.3.1 The Experimental Layout

0.2% (by atom) H_2O comtamination. The ionic content was enhanced by making a solution of solium peroxide with the deuterium oxide. The resulting gas was analysed by means of a mass spectrometer. The hydrogen contamination was found to be 0.3% to 0.4% although, due to calibration difficulties in the low mass region, the reliability of this measurement is questionable. Thus the gas was taken to have a 0.3% hydrogen contamination.

Beam particles which did not stop in the target were vetoed by the plastic scintillator C3. With this arrangement we stopped 25% to 50% of the incident pion beam in the target liquid. The scintillators in the pion beam were hidden from the NaI detectors with lead shielding to reduce the contribution of charge exchange in hydrogen to a minimum. The plastic scintillators C4, C5, and C5' served as charged particle tags to distinquish electrons from the γ-rays entering the spectrometers.

A stopped pion was defined by the coincidence condition $C1 \cdot C2 \cdot \overline{C3}$. An event was defined by the coincidence of a stopped pion and a signal from either TINA (T) or MINA (M). That is an event was defined as $C1 \cdot C2 \cdot \overline{C3} \cdot (T + M)$. The pion stop rate was typically 2×10^4 sec^{-1} and the event rate was about 60 sec^{-1}.

4. Electronics and Data Collection

Figure II.4.1 is the schematic of the electronics. The outputs of the TINA and MINA phototube bases were brought separately into the counting room on low loss cables (FM-8) to allow the phototube gains to be balanced. The signals were then summed in active fan-in modules (LRS 127B, LRS 428) inside the counting room. The summed spectrometer signals were split in isolated output fanout modules (LRS 128) and processed for pulse height and timing information. All of the data was digitized in CAMAC modules interfaced through a standard CAMAC crate to a PDP-11-40 computer. The pulse height information was processed in two channels of the LRS octal ADC (model 2248). The timing information was processed in two channels of an LRS octal TDC (model 2228). Since we are interested in examining only "events" it was necessary to start the TDC with the "event" signal. Because the timing quality of this signal was poor a third TDC channel was used to record the time of passage of the pion through C2 as a zero time reference. Hence the relevant times are $t_{TINA} - t_{C2}$ and $t_{MINA} - t_{C2}$. The timing of all three stop signals was done with constant fraction discriminators (Ortec 463). The charged particle tags C4 and C5 + C5' were fed into CAMAC scalers and a charged particle was identified by a non-zero count in the appropriate scaler. In addition CAMAC scalers were used to record the number of π^- stops and the number of events observed.

Once an event had been accepted by the CAMAC - PDP-11-40 computer system no further events could be accepted until that event had been processed by the software. Although the time required to accomplish this varied considerably depending upon the type of event this time did not exceed 10^{-3} sec. Thus the dead time for an event rate of 60 sec^{-1} was less than 6%. The software processing involved two stages. First the

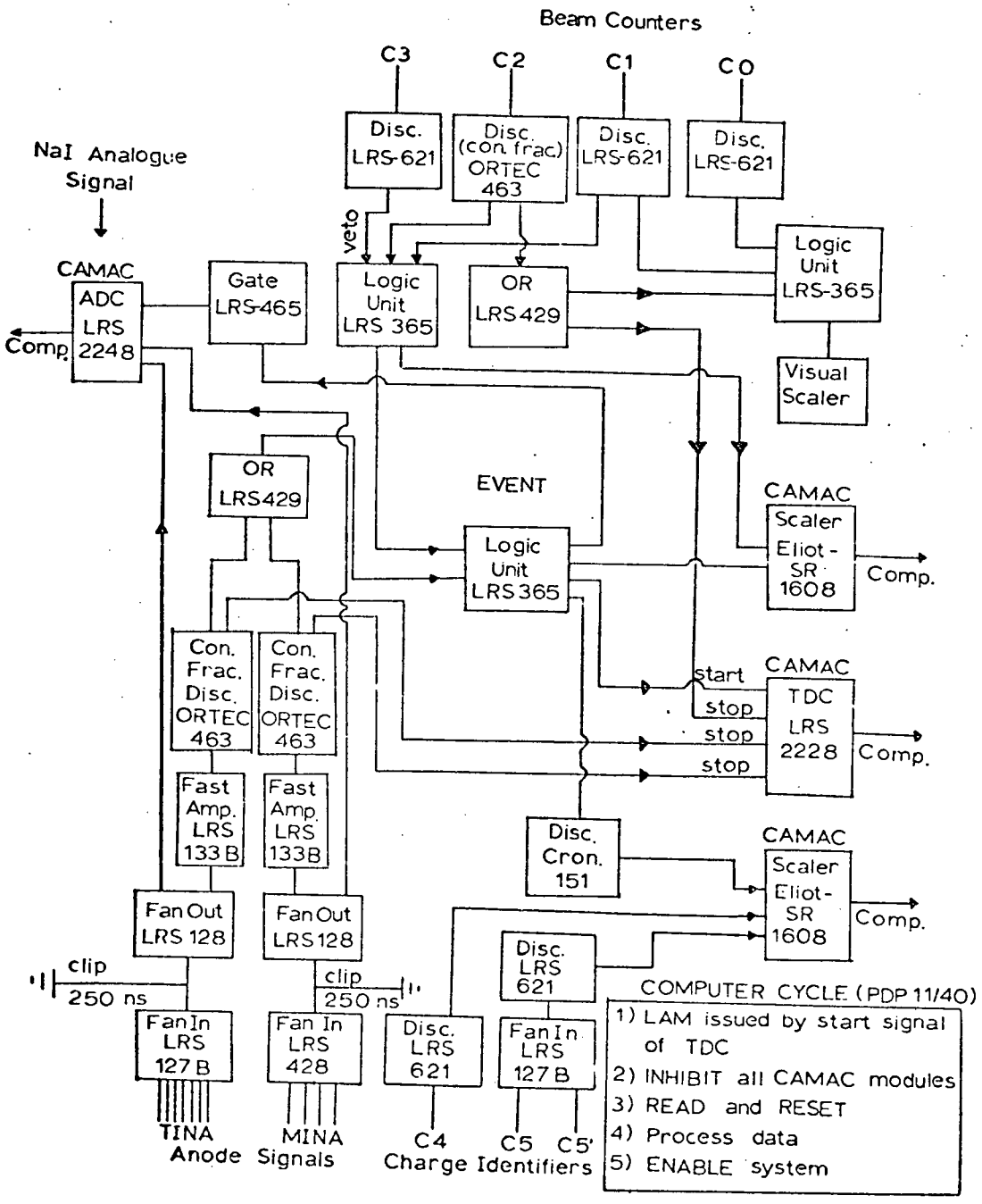
Beam Counters
C3
C2
C1
C0
Disc. LRS-621
Disc. (con. frac.) ORTEC 463
Disc. LRS-621
Disc. LRS-621
NaI Analogue Signal
veto
CAMAC
ADC LRS 2248
Comp.
Gate LRS-465
Logic Unit LRS 365
OR LRS429
Logic Unit LRS-365
Visual Scaler
OR LRS429
EVENT
CAMAC
Scaler Eliot-SR 1608
Comp.
Logic Unit LRS365
Con. Frac. Disc. ORTEC 463
Con. Frac. Disc. ORTEC 463
start
stop
stop
stop
CAMAC
TDC LRS 2228
Comp.
Fast Amp. LRS 133B
Fast Amp. LRS 133B
Disc. Cron. 151
CAMAC
Scaler Eliot-SR 1608
Comp.
Fan Out LRS 128
Fan Out LRS 128
clip
250 ns
clip
250 ns
Disc. LRS 621
Fan In LRS 127B
Fan In LRS 428
Disc. LRS 621
Fan In LRS 127B
TINA Anode Signals
MINA
C4 Charge Identifiers
C5
C5'
COMPUTER CYCLE (PDP 11/40)
1) LAM issued by start signal of TDC
2) INHIBIT all CAMAC modules
3) READ and RESET
4) Process data
5) ENABLE system

event was analysed and binned into time and energy histograms and second, the event was recorded on magnetic tape for a more complete off-line analysis.

In the on-line analysis seven one-dimensional 256 channel histograms were formed. These were the TINA/MINA time spectra, the TINA/MINA γ-ray energy spectra, the time difference spectrum ($T_{TINA} - T_{MINA}$) and the TINA/MINA coincident γ-ray energy spectra. In addition one two dimensional 64 x 64 channel histogram was formed. The axes were the TINA coincidence γ-ray energy and the MINA coincidence γ-ray energy.

The data recording was done on Dectape and later the data were transferred to IBM compatible 9 track magnetic tape. The Dectape has the disadvantage of being a rather inefficient medium for storage of a large amount of data and because we had only a finite number of these small tapes the data recording had to be done selectively. Two modes of data recording were used. In the "singles" recording mode events were selected on the basis of their time of flight; data for neutrons not being recorded. In general the recording threshold was set well into the neutron time of flight peak to ensure that all γ-rays were recorded. In one run all neutron events in TINA were recorded. In the "coincidence" recording mode only coincident events were recorded but, with the exception of one run, neutron coincidences as well as gamma ray coincidences were recorded.

5. Summary

The data were taken over a period of about 68 hours beginning on May 28, 1976. The data were recorded in 11 runs of singles recording mode and 6 runs of coincidence recording mode. Except for one case in which two short coincidence recording runs were taken consecutively the coincidence recording runs were alternated with singles recording runs. This was done to minimize the effect of gain and zero shifts in the pulse height data. A total of 2.2×10^9 π^- stops and 6,153,962 events were observed. Of these half were observed during singles recording runs and half during coincidence recording runs.

CHAPTER III

THE DATA ANALYSIS

1. The Off-line Analysis

Because the data were recorded on magnetic tape it was possible to do a more refined data analysis than that provided by the on-line computer. In particular it was possible to apply gain and zero channel stabilization to the data during the re-analysis and thereby significantly improve the energy resolution. It was also possible to generate various histograms which were not available in the on-line analysis and to adjust the definition of γ-rays and neutrons on the basis of the time spectra. The time spectra of TINA and MINA for a single run are shown in figure III.1.1 with the time definition of the γ-rays marked. As can be seen there was good separation between the neutrons and γ-rays in TINA and the overlap may be considered to be negligible. In MINA the separation was not quite as good. This was partially due to the smaller distance from the target and partially due to an increased peak width. TINA was 122.9 cm. from the center of the target and there was a time separation of 7.2 nsec. between the γ-rays and the high energy neutrons. MINA was 103.2 cm. from the target center giving a time separation of 6.1 nsec. These times are indicated on figure III.1.1 and are seen to be consistent with the leading edge of the neutron peak. The increased width of the MINA γ-ray peak can be understood in terms of the low gain on the primary dynode stages of the photomultiplier tubes. This same problem also resulted in poor energy resolution in the MINA spectrometer. Even with the reduced separation in MINA the overlap of neutrons and γ-rays was negligible.

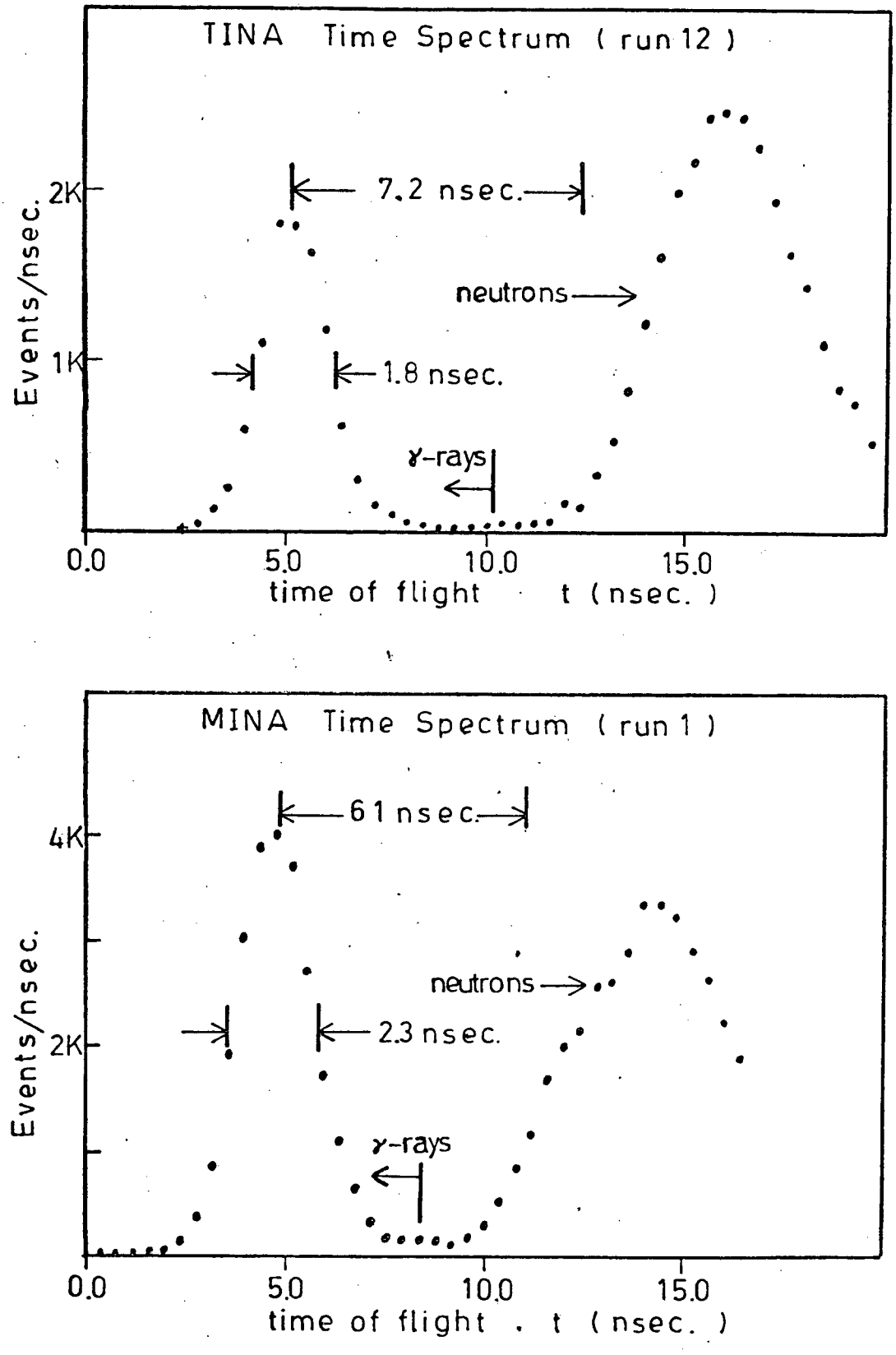

Figure III.1.1 Typical NaI Time Spectra

The energy spectra of the singles Υ-rays in TINA and MINA are shown in figure III.1.2. In the TINA spectrum there is an obvious shoulder at 55 MeV due to the charge exchange box spectrum from the small hydrogen content of the target. As mentioned earlier deuterium charge exchange Υ-rays comprise only 3% of the events in this region. The high energy edge of the box spectrum is hidden in the rapidly rising radiative capture spectrum. In the MINA spectrum the energy resolution was not sufficient to see any indication of the charge exchange box spectrum.

It has been mentioned previously that there were problems with gain and zero stability over the duration of the experiment. The extent of the problem is seen by examining the zero point energies and radiative capture centroids for individual runs. These values are plotted as a function of run number in figure III.1.3. The curve drawn on these points serves only to guide the eye. One would expect that the width of a peak would be increased by at least an amount comparable to the zero shift. In TINA this was about 4 MeV and in MINA 7 MeV. This was a serious problem in view of the small energy separation between the hydrogen and deuterium charge exchange lineshapes (about 5 MeV).

One of the beauties of an experiment which records raw data from events on magnetic tape is that it is possible to compensate for this type of problem in a dynamic way. In order to do this the energy parameters were re-defined as:

$$E_T' = G_T(E_T - Z_T) \quad ,$$

$$E_M' = G_M(E_M - Z_M) \quad ,$$

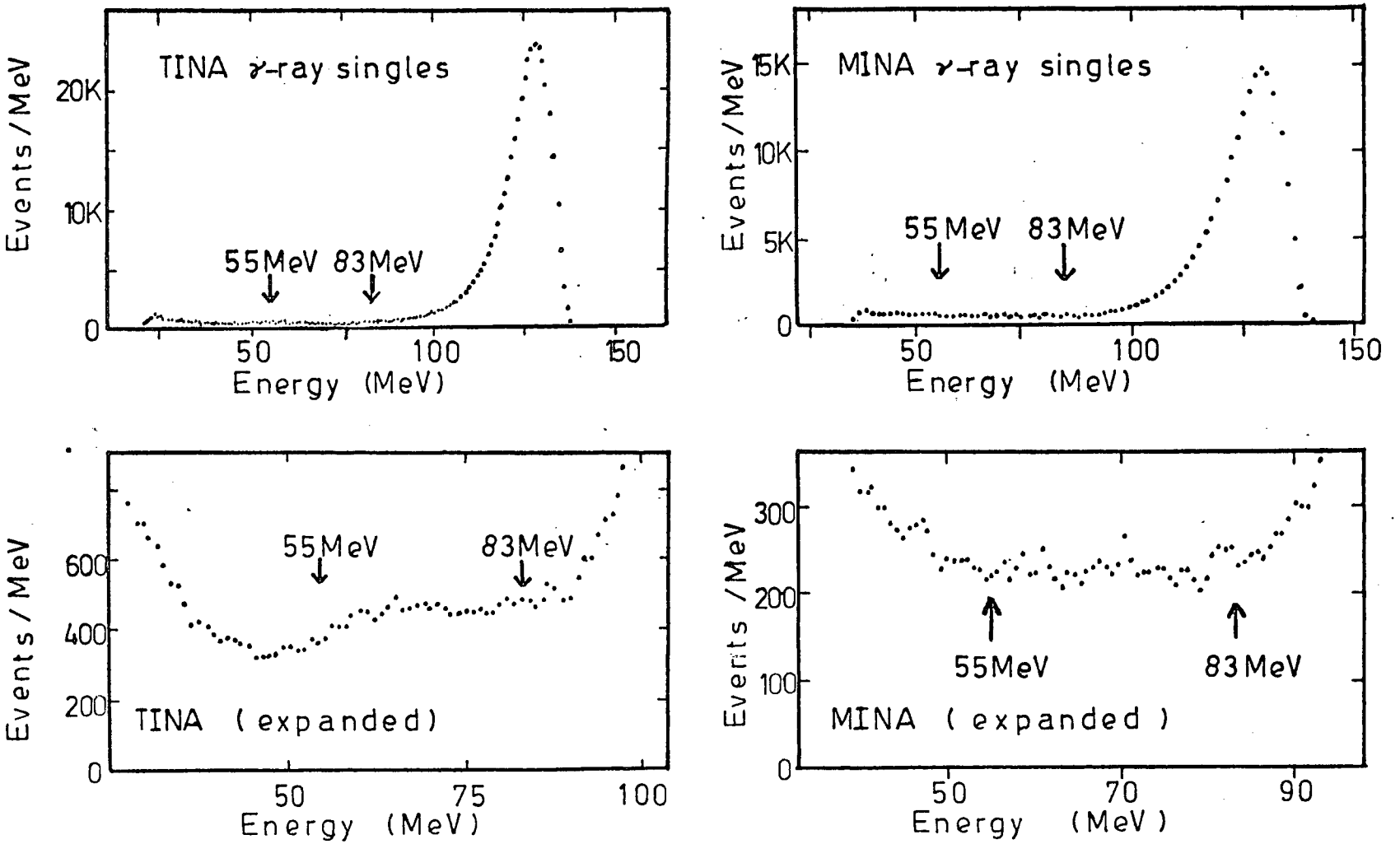

Figure III.1.2 Radiative Capture γ-rays from Deuterium

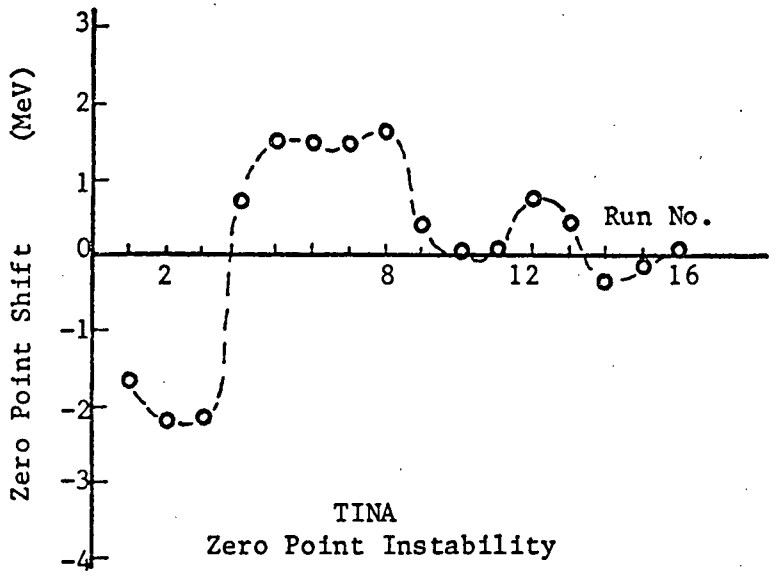

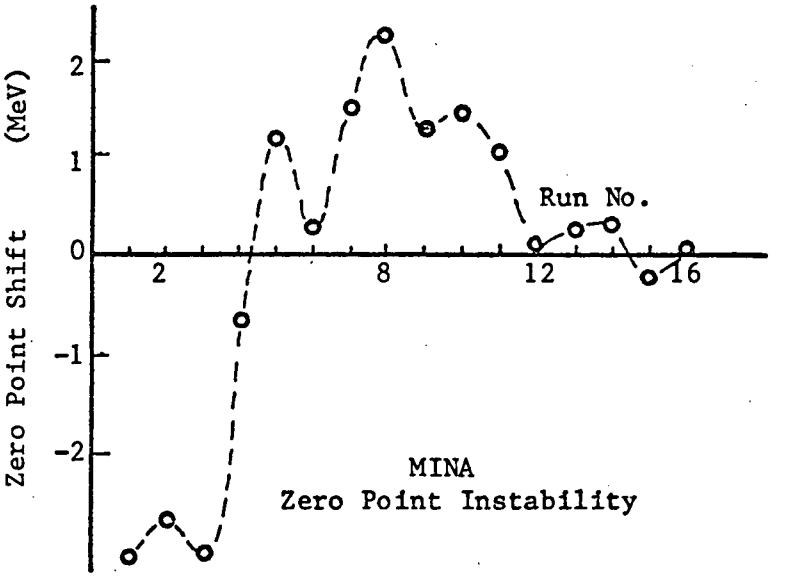

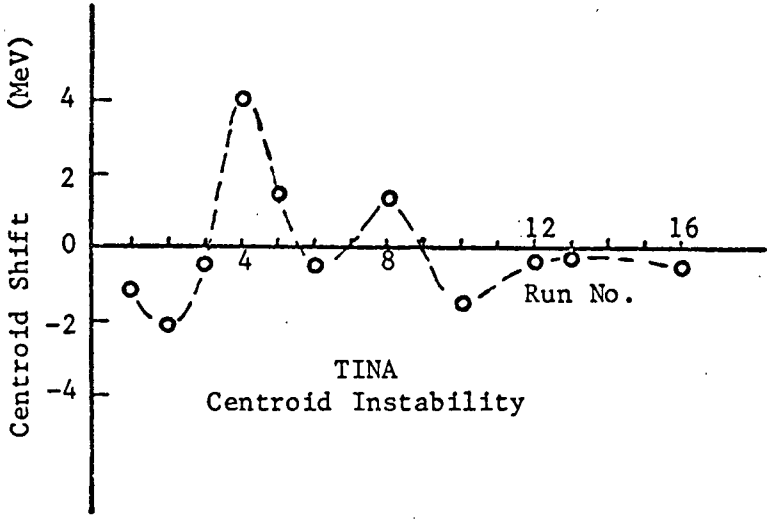

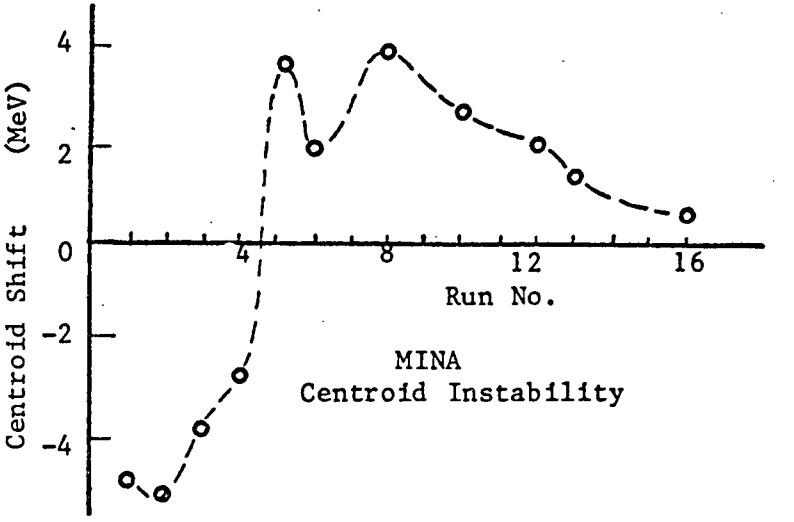

Figure III.1.3 Centroid and zero point instabilities in TINA and MINA

where E_T and E_M are the energy data for TINA and MINA recorded for a particular event. Z_T and Z_M are zero point adjustments associated with TINA and MINA respectively and G_T and G_M are adjustable gain factors. Dynamic gain stabilization was achieved by continuously modifying the gain and zero parameters in such a way as to correct for the gain and zero shifts in the original data. It was necessary to define the centroid energies (C^o) and zero point energies (Z^o) which were to be maintained. The choice of these values is entirely arbitrary. However once they have been determined the gain (G) and zero (Z) parameters should be chosen so that the initial centroid and zero point energy of the data will correspond to the chosen fixed values (C^o and Z^o). The fixed zero energies were taken to be

$$Z_T^o = 0.0 \quad \text{(channel number)} ,$$

$$Z_M^o = 0.0 \quad \text{(channel number)} ,$$

The initial zero parameters were then chosen as the average zero point energy of run #1;

$$Z_T = 19.03 \quad \text{(channel number)} ,$$

$$Z_M = 7.62 \quad \text{(channel number)} ,$$

The fixed centroid energies were taken to be the average centroid position for run #1 corrected for the initial zero parameters (Z_T and Z_M);

$$C_T^o = 132.27 \quad \text{(channel number)} ,$$

$$C_M^o = 173.54 \quad \text{(channel number)} .$$

With these values for the fixed centroid energies the appropriate choices for the initial values of the centroid parameters (C_T and C_M) were

$$C_T = C_T^o \quad , \quad C_M = C_M^o .$$

The gain parameters were defined to be

$$G_T = \frac{C_T^o}{C_T} \quad ; \quad G_M = \frac{C_M^o}{C_M} \quad .$$

Hence the initial value of the gain parameters was 1.0.

A γ-ray event was recognized as a high energy γ-ray if E' was within one half width at half-maximum of the fixed centroid energy. For such events the centroid parameter was adjusted by an amount ΔC where

$$\Delta C = k_c (E' - C) ,$$

k_c being a small ($<< 1$) constant, and the gain was re-defined with the new value of C.

$$G = \frac{C^o}{C} \quad .$$

Except in the case of a coincidence event zero energy events were available for one spectrometer when the event was the result of a response in the opposite spectrometer. Because there was no "stop" signal for such events they could be recognized by an overflow in the corresponding time data. For zero energy events the zero parameter was adjusted by an amount ΔZ,

$$\Delta Z = k_Z(E - Z) \ ,$$

where k_Z is a small ($<<1$) constant. Of course the adjustments were applied after the event itself had been analysed to avoid any auto-biasing effects. Suitable values for k_c and k_z were found to be 10^{-3} and 10^{-4} respectively. The variation of the parameters was monitored as the stabilized analysis was done. The results are plotted in figure III.1.4. The indication from these graphs is that for both TINA and MINA most of the observed fluctuation was due to the zero shift. The effectiveness of the stabilization may be measured by comparing the centroid positions for individual runs with and without the stabilization. These centroid positions have been plotted in figure III.1.5. In TINA the improvement is seen to be a factor of 3. In MINA the improvement is more than a factor of 2. The residual differences in centroid position among the runs were corrected by stretching all of the spectra to give them a common centroid. The same stabilization and stretching procedure was applied in the case of the coincidence spectra. The usefulness of this procedure is clearly seen in the improvement of the TINA coincidence spectrum (figure III.1.6). The MINA coincidence spectrum is also shown

here and it is seen that the separation between the hydrogen and deuterium charge exchange events is still very poor.

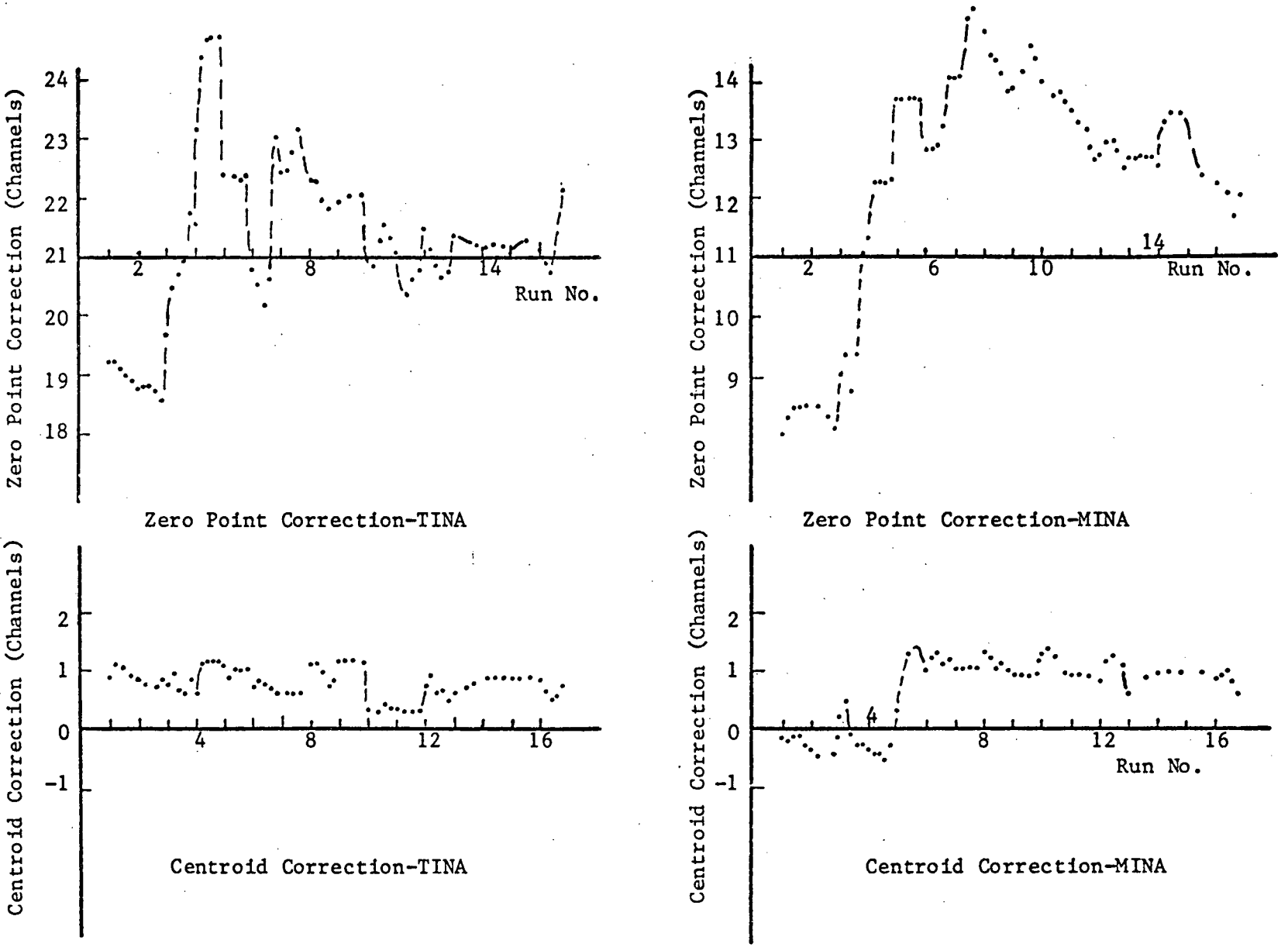

Figure III.1.4 Centroid and Zero Point Corrections in TINA and MINA

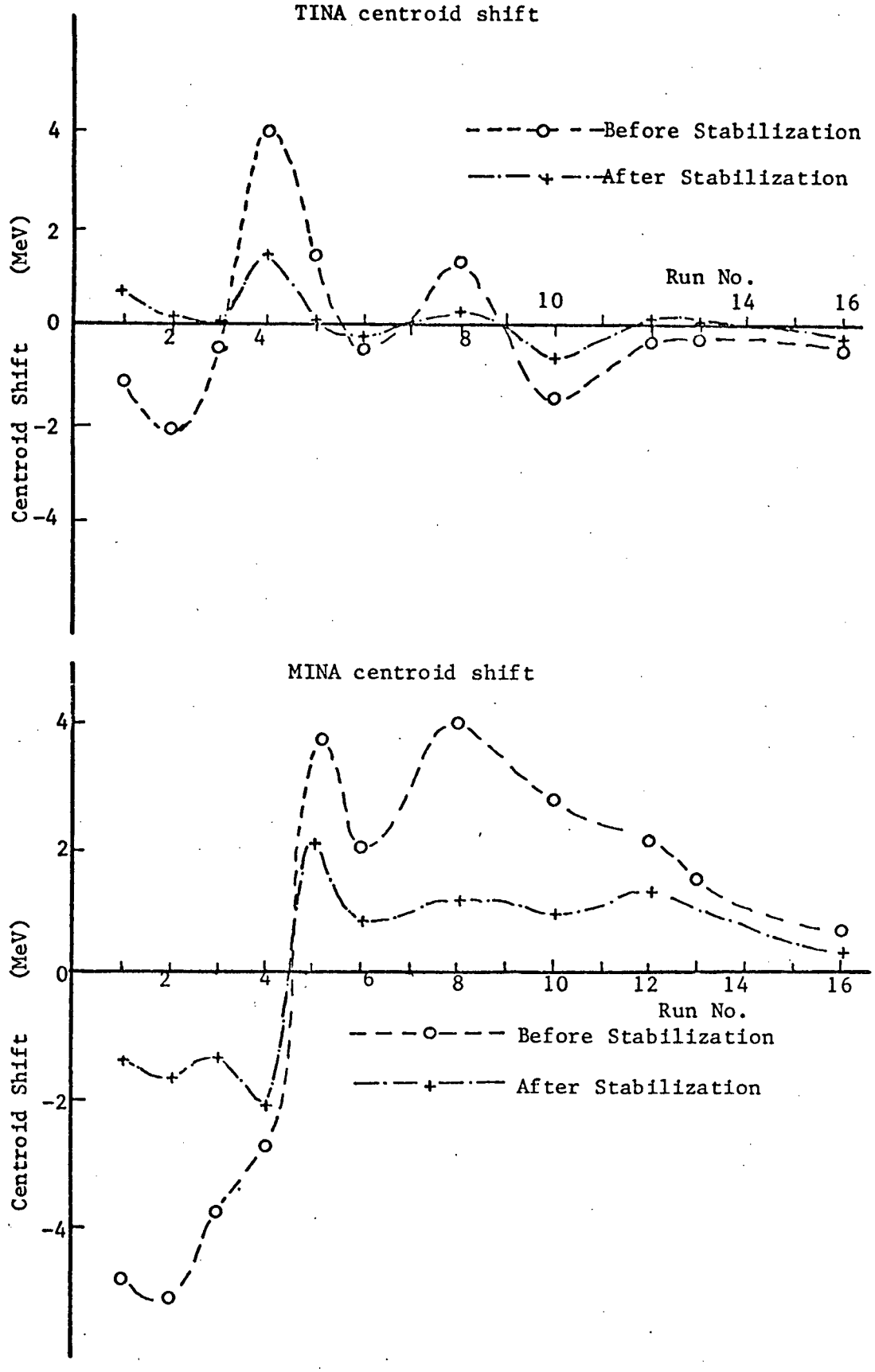

Figure III.1.5 Effect of Gain and Zero Stabilization

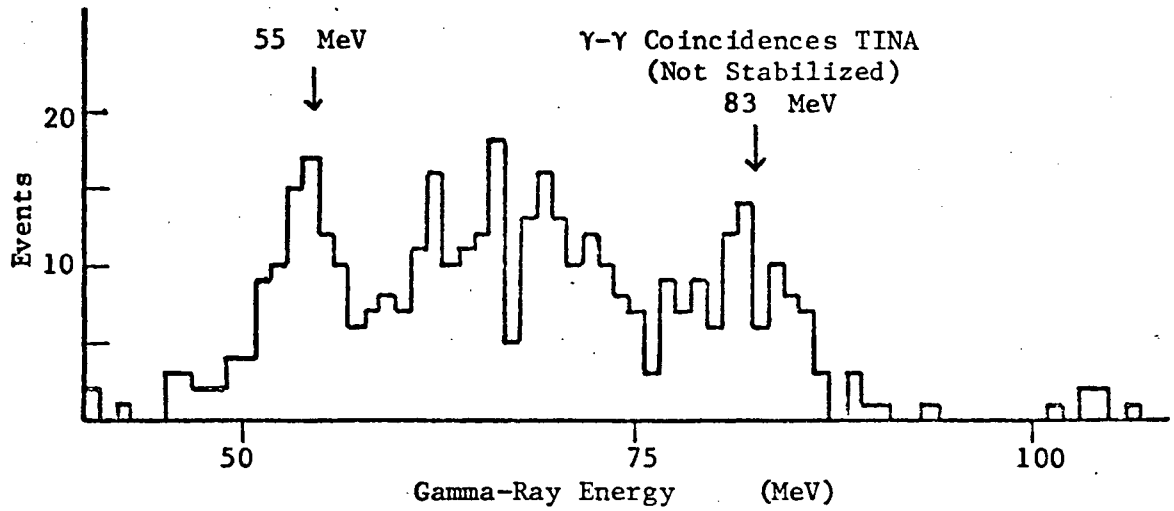

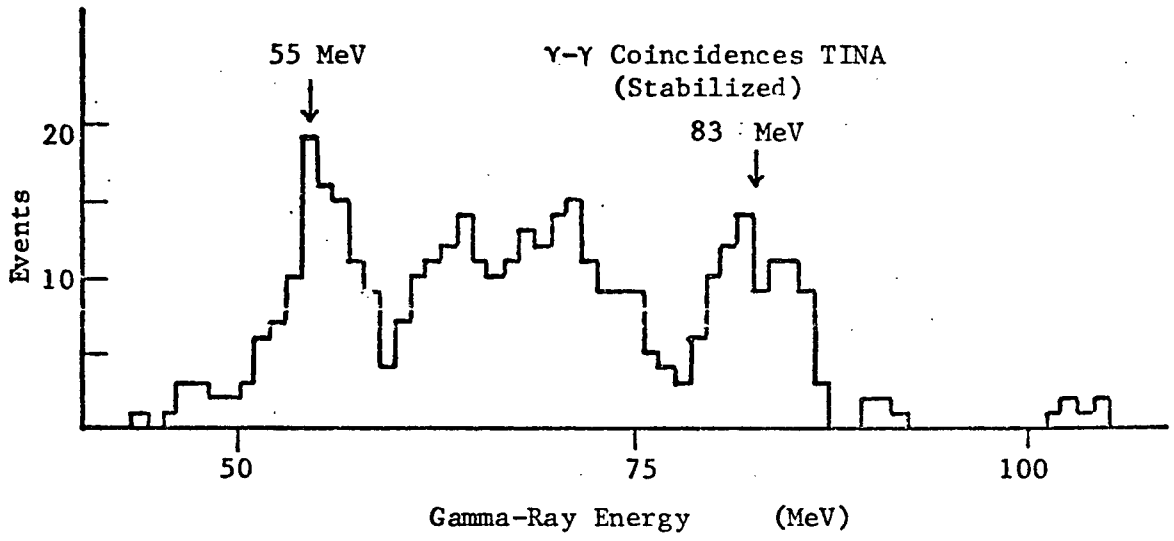

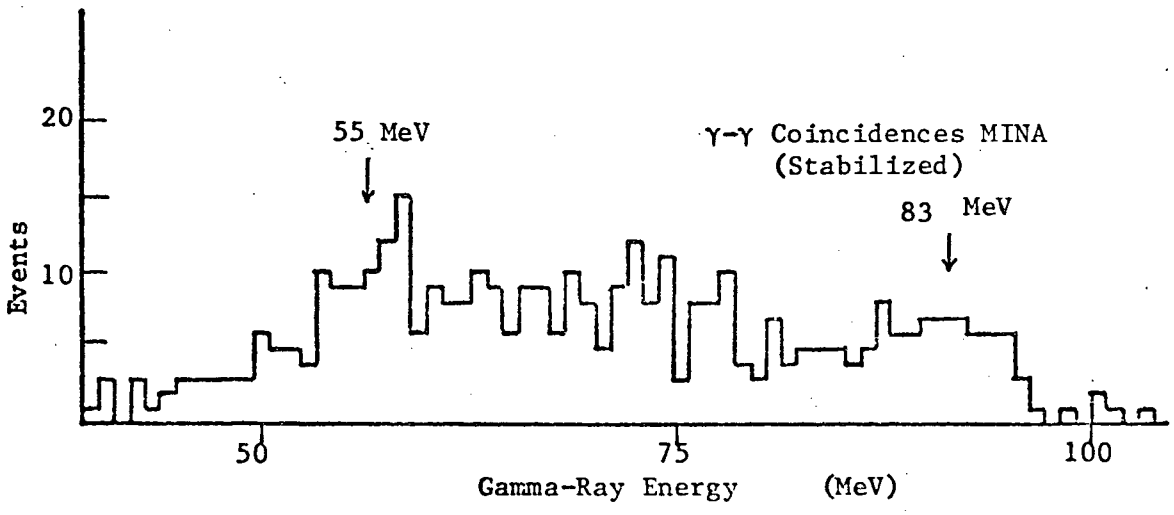

Figure III.1.6 Gamma-Ray Coincidence Spectra

2. Fitting the Histograms

Two procedures were used to determine the branching ratio for charge exchange in deuterium. The first was the comparison of the number of deuterium charge exchange coincidences to the number of radiative capture events tempered with the relative efficiencies for observing these processes.

$$R_1 = \frac{D_\pi}{\xi_{\pi D}} \frac{\xi_S}{N\gamma(\pi^- d \rightarrow \gamma nn)} \frac{1}{S + 1} \qquad \text{(III.2.1)}$$

where:

D_π is the number of coincidence γ-rays due to charge exchange in deuterium

$\xi_{\pi D}$ is the efficiency for observing deuterium charge exchange coincidence γ-rays

ξ_S is the efficiency for observing singles γ-rays

$N\gamma(\pi^- d \rightarrow \gamma nn)$ is the number of radiative capture γ-rays observed.

The second approach was the comparison of the relative number of charge exchange events due to deuterium and due to hydrogen. The charge exchange branching ratio in deuterium may then be calculated from the known charge exchange branching ratio in hydrogen if the effective concentration of hydrogen in the target is known.

$$R_1 = R_H C_H \frac{D_\pi}{\xi_{\pi D}} \frac{\xi_{\pi H}}{H_\pi} \qquad \text{(III.2.2)}$$

where

R_H is the charge exchange branching ratio in hydrogen

C_H is the effective concentration of hydrogen in the target

H_π is the number of coincidence γ-rays due to charge exchange in hydrogen

$\xi_{\pi H}$ is the efficiency for observing hydrogen charge exchange coincidence γ-rays.

The effective concentration of hydrogen in the target was not trivial to determine. First, the concentration of hydrogen in the gas was expected to be reduced in the liquid state due to distillation. (The boiling point of hydrogen is about 3.2K lower than that of deuterium at normal pressures (MC64). A second possible effect was the preference of stopped π^- captured in molecular H-D orbits to form π^--D atomic states rather than π^--H atomic states. The effect of preferential π^- capture on high Z nuclei in hydrogenous compounds is well known (KR68, PE69, PO73). In the case of deuterium hydride (H-D) the π^- bound states are slightly deeper ($\simeq$6%) on the deuteron than on the proton. These effects which reduce both the effective concentration of hydrogen in the liquid and the actual concentration in the liquid from the concentration in the gas are discussed more fully in Appendix IV. It was possible to directly measure the effective hydrogen concentration in the target liquid by examining the singles spectrum for charge exchange events.

In summary it was necessary to extract the numbers D_π and H_π from the γ-ray coincidence spectrum and a value for C_H from the γ-ray singles spectrum.

A. The Coincidence Spectrum

Even with stabilization to correct the gain and zero shifts the coincidence γ-rays from hydrogen charge exchange still encroach significantly into the region of the deuterium charge exchange events. In order to extract the number of deuterium events and the number of hydrogen events from the coincidence spectrum the hydrogen component was fit with an empirical hydrogen coincidence lineshape. This lineshape was measured in conjunction with a re-measurement of the Panofsky ratio in hydrogen (SP77). The geometry of the two experiments was identical except for a 3% difference in the distance of the TINA collimator from the target (113.0 cm. instead of 110.2 cm.). The fit of the empirical lineshape is shown superimposed on the TINA coincidence data in figure III.2.1. It can be seen to give a very good fit to the hydrogen charge exchange peaks. In fitting the amplitude of the empirical function it

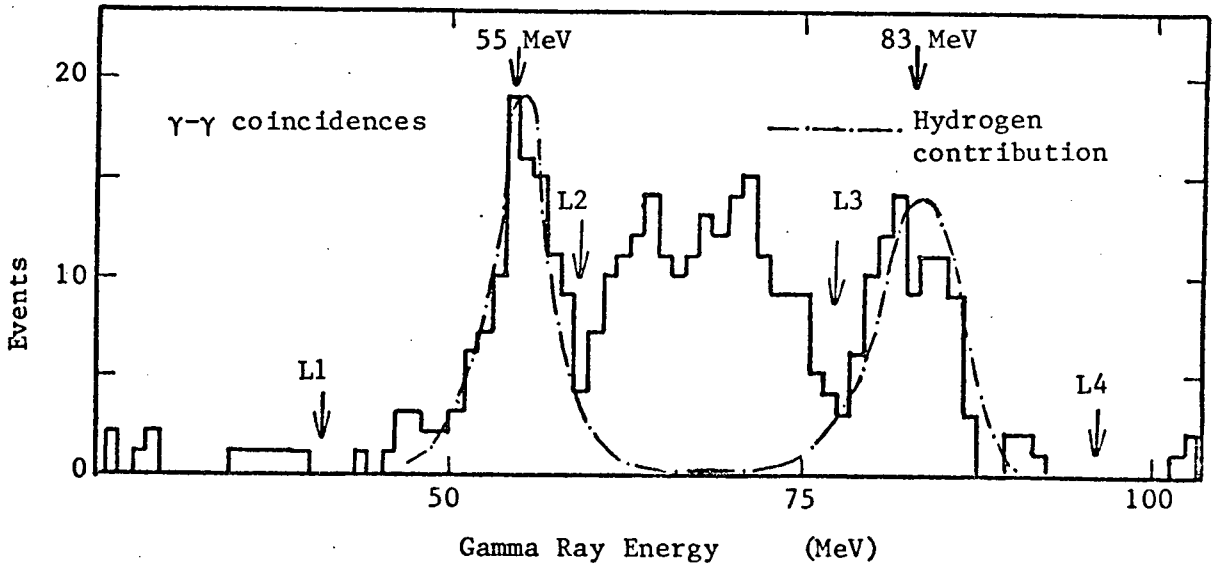

Figure III.2.1 - Fit of the Hydrogen Peaks

was important to not consider the events due to deuterium charge exchange. Hence the central region was omitted from the fitting procedure and only the regions shown as (L_1,L_2) and (L_3,L_4) on figure III.2.1 were considered. To test the effect of any deuterium events in these regions the limits L_2 and L_3 were varied over a wide range of energies and the effect of the fit was observed. In figure III.2.2 the amplitude of the empirical lineshape is plotted as a function of the values L_2 and L_3. As expected there was negligible variation of the amplitude with variations of the exterior limits. The slight variations in the amplitude with the variation of the interior limits, L_2 and L_3, are seen to be well within the error limits set for the amplitude. We conclude that the dependence of the fit upon these parameters and upon any deuterium events in the regions defined by these parameters is negligible. In the region between the limits L_2 and L_3 there were 182.0 ± 13.5 events of which we determine 22.2 ± 2.3 were due to charge exchange in hydrogen. This leaves 159.8 ± 13.7 events in this region due to charge exchange in deuterium. The number of deuterium events under the hydrogen peaks was determined by subtracting the fit in these regions from the data. The result was that there are 8.2 ± 14.5 deuterium events under the hydrogen peaks. Thus the total number of deuterium charge exchange events in the coincidence spectrum was 168.0 ± 20. The total number of events from hydrogen charge exchange was determined directly from the fit to be 195.6 ± 15.6 where the error includes the statistics of the empirical spectrum.

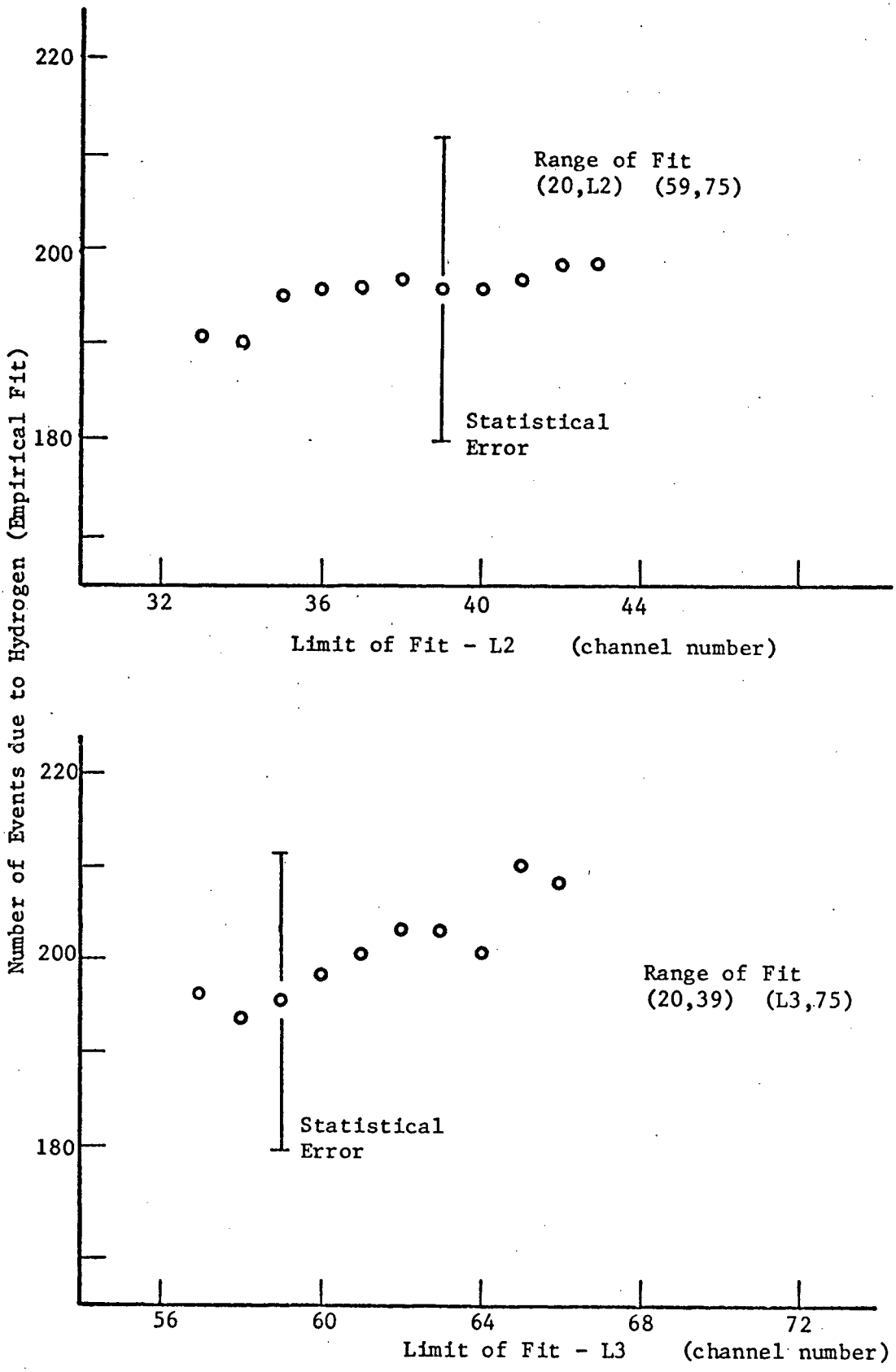

Figure III.2.2 Estimated Number of Hydrogen γ-ray coincidences as a function of the range of the fit.

B. The Singles Spectrum

To extract the number of charge exchange γ-rays from the TINA singles γ-ray spectrum the data were fitted in the region between 20 MeV and 95 MeV with a smooth estimate of the background and γnn tail (f(E)) and an empirical charge exchange γ-ray spectrum from hydrogen (g(E)). The hydrogen charge exchange spectrum used is shown in figure II.1.2. The experimental configuration of the hydrogen target and the TINA spectrometer was the same for the present experiment except for a 3% difference in the distance separating them (113.0 cm. compared with 110.2 cm. in the present case). The function used to fit the background was

$$f(E) = ae^{bE} + \sum_{i=0}^{3} c_i E^{-i} + dg(E).$$

The first term was included to approximate the radiative capture γ-ray tail. The second term was included to fit the rising low energy background. The last term represents the contribution of charge exchange events to the spectrum in this region. A grid search technique for the parameter b was combined with a linear least squares technique for parameters a, c and d. The data and the fitting functions are shown in figure III.2.3a. Figure III.2.3b shows the difference between the data and the fit. The parameter 'd' was tested for its dependence upon the limits of the fitting range and upon different choices of f(E). The value of 'd' was found to be relatively independent of the high energy limit of the fitting range but dependent upon the low energy limit (figure III.2.4). Good fits to the data were achieved for any inverse polynomial of second order or larger and the order had little influence

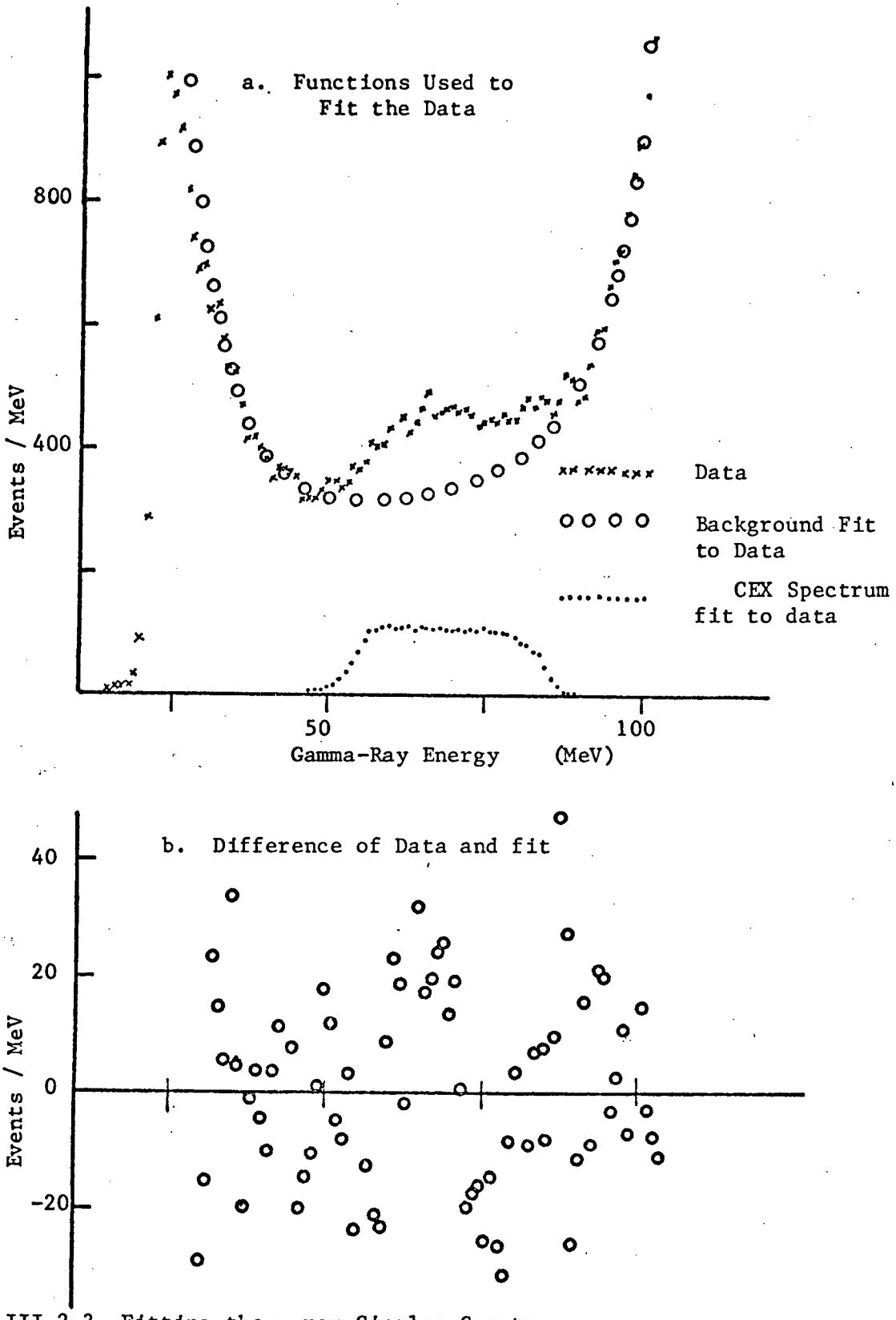

Figure III.2.3 Fitting the γ-ray Singles Spectrum

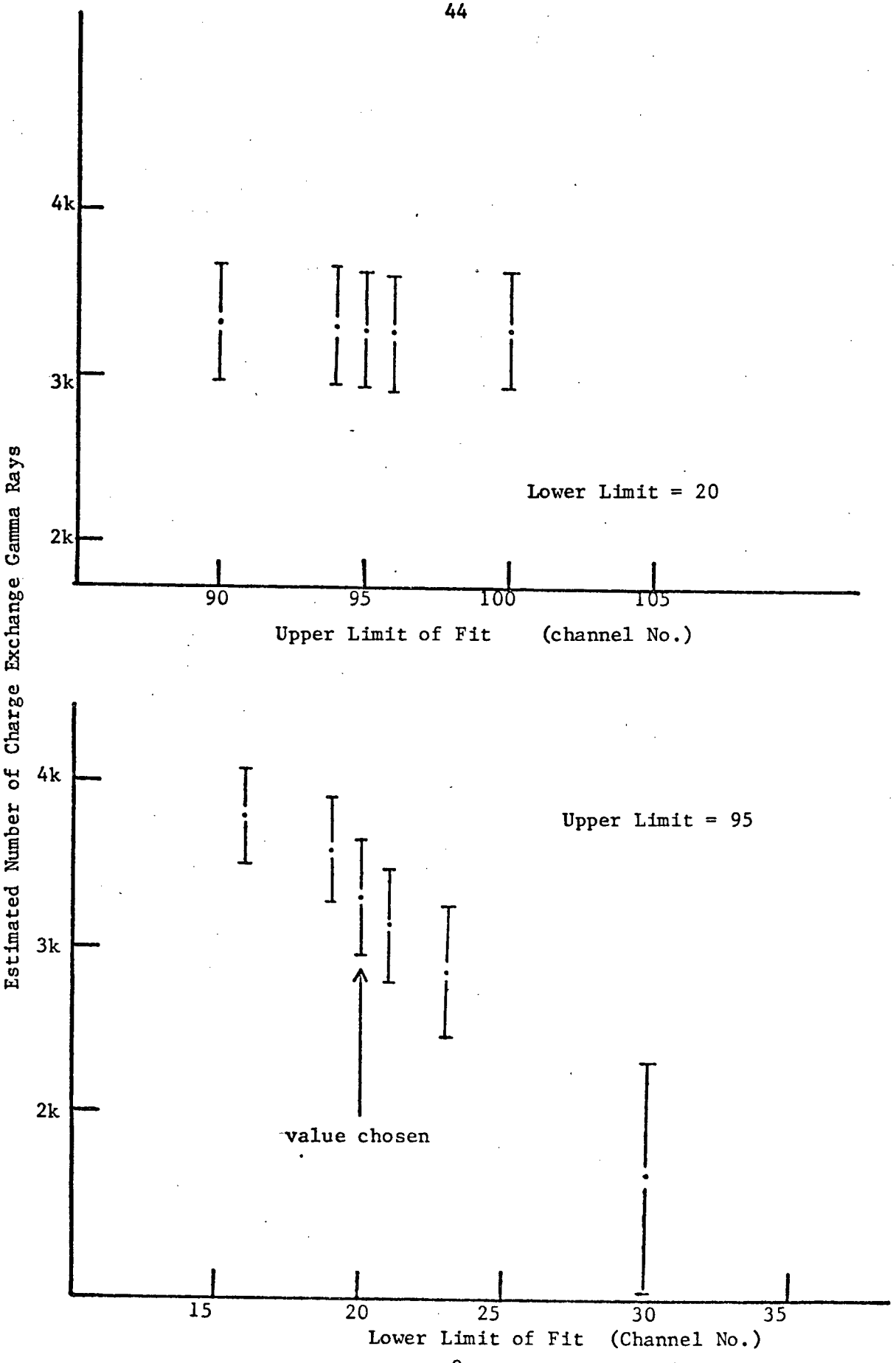

Figure III.2.4 Estimated Number of π^0 Singles γ-rays as a Function of the range of fit

upon the parameter 'd'. Inclusion of positive powers of energy in the polynomial was found to give generally unsatisfactory fits to the data as evidenced by significant structure in the difference between the fit and the data. The final value of the parameter 'd' was

$$d = 0.0190 \pm 0.0035.$$

The error was assigned largely on the basis of the variation of the parameter with the low energy limit of the fitting range.

The effective concentration of hydrogen (i.e. the relative proportion of π^- which are captured by hydrogen atoms), C_H, may be determined from the number of singles γ-rays from hydrogen and deuterium.

$$C_H = \frac{C_D}{2} \frac{N_\gamma(\pi^- p \rightarrow \pi^o n)}{N_\gamma(\pi^- d \rightarrow \gamma nn)} \frac{1}{P_H(S+1)}$$

where

C_D is the concentration of deuterium, taken as 1.0

$N_\gamma(\pi^- p \rightarrow \pi^o n)$ is the number of γ-rays from π^- charge exchange on hydrogen

$N_\gamma(\pi^- d \rightarrow \gamma nn)$ is the number of γ-rays from π^- radiative capture on deuterium.

The charge exchange γ-rays in the singles spectrum are due to both charge exchange in hydrogen and charge exchange in deuterium. The number of singles γ-rays due to charge exchange in hydrogen may be extracted by referring to the coincident γ-ray spectrum (figure III.2.1) from which the ratio

$$F = \frac{N_\gamma(\pi^- d \rightarrow \pi^0 nn)}{N_\gamma(\pi^- p \rightarrow \pi^0 n)} = \frac{D_\pi}{\xi_{\pi D}} \frac{\xi_{\pi H}}{H_\pi}$$

may be determined. Then the number of singles γ-rays due to hydrogen is just

$$N_\gamma(\pi^- p \rightarrow \pi^0 n) = \frac{N_\gamma(\pi^- p \rightarrow \pi^0 n) + N_\gamma(\pi^- d \rightarrow \pi^0 nn)}{F + 1}$$

Using the values for the efficiencies presented in chapter III.3 and the final values of D_π and H_π presented in chapter III.5 we find

$$F = 0.132 \pm 0.020,$$

$$N_\gamma(\pi^- p \rightarrow \pi^0 n) = 2911 \pm 585,$$

$$C_H = 0.00145 \pm 0.00029 .$$

Thus the effective concentration of hydrogen is found to be reduced by a factor of two from the nominal concentration of 0.3%.

3. The Coincidence Efficiency

Because the reactions take place at rest the γ-rays are isotropically distributed in the lab frame. The singles efficiency is then simply the solid angle factor for the collimator of the spectrometer. For TINA

$$\xi_s(T) = (3.29 \pm 0.03) \times 10^{-3}$$

and for MINA

$$\xi_s(M) = (2.11 \pm 0.02) \times 10^{-3}$$

The efficiency calculation for coincidence γ-rays is somewhat more involved due to the correlation between the direction of the two γ-rays. It is shown in appendix I.3 that for a π^o of total energy E_π and momentum P_π and first γ-ray of energy E_γ the second γ-ray must lie on the surface of a cone of half-angle ϕ_1,

$$\cos\phi_1 = \frac{E_\gamma^2 + (E_\pi - E_\gamma)^2 - P_\pi^2}{2E_\gamma(E_\pi - E_\gamma)} \qquad \text{(III.3.1)}$$

whose axis is the direction of the first γ-ray. For a fixed direction and energy of the first γ-ray the efficiency for detecting the second γ-ray is determined by the amount of the γ-ray cone which intersects the collimator. In figure III.3.1 we consider the case of a π^o decay on the axis of the spectrometers.

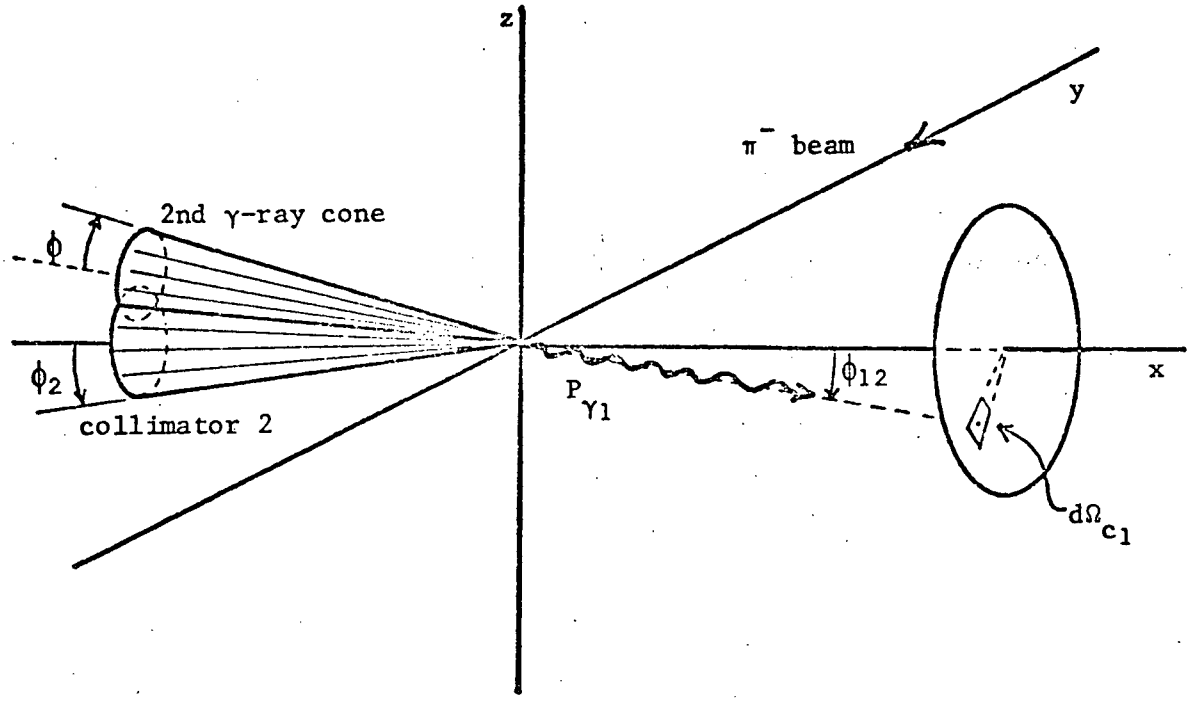

Figure III.3.1 π^o Decay on the Collimator Axis

The probability for detecting a coincidence can be shown (appendix II) to be

$$dP_c = \frac{1}{2\pi^2} \cos^{-1}\left(\frac{\cos\phi_2 - \cos\phi_1\cos\phi_{12}}{\sin\phi_{12}\sin\phi_1}\right) \frac{dN_\gamma}{dE_\gamma} \frac{dN_\pi}{dT_\pi} d\Omega_{c_1} dE_\gamma dT_\pi \qquad \text{(III.3.2)}$$

where ϕ_1 is determined by (III.3.1), ϕ_2 and ϕ_{12} are determined by the geometry (figure III.3.1), $\frac{dN_\gamma}{dE_\gamma}$ is the charge exchange singles γ-ray (box) spectrum (AI.2.1) and $\frac{dN_\pi}{dT_\pi}$ is the π^o energy spectrum. In the case of charge exchange in hydrogen the π^o is monochromatic. Hence

$$\frac{dN_\pi}{dT_\pi}(p) = \delta(T_o - T_\pi)$$

where T_o = 2.90 MeV is the kinetic energy of the π^o. In the case of deuterium the π^o has a continuous energy spectrum from 0 MeV to T_{MAX} = 1.1 MeV given by (Appendix III)

$$\frac{dN_\pi}{dT_\pi}(D) = \left(\frac{T_\pi}{T_{\pi MAX}}\right)^{3/2} \left(1 - \frac{T_\pi}{T_{\pi MAX}}\right)^{3/2}$$

The net probability of detecting a coincidence γ-ray of energy E_γ, i.e. the coincidence lineshape is just the 3-fold integration

$$\mathcal{L}(E_\gamma) = \frac{dP_c}{dE_\gamma} = \int_{T_\pi} \int_{\Omega_c} \frac{1}{2\pi^2} \cos^{-1}\left(\frac{\cos\phi_2 - \cos\phi_1\cos\phi_{12}}{\sin\phi_{12}\sin\phi_1}\right) \frac{dN_\gamma}{dE_\gamma} \frac{dN_\pi}{dT_\pi} d\Omega_c dT_\pi \qquad \text{(III.3.3)}$$

The net probability for detecting a coincidence γ-ray of any energy is the further integration,

$$\xi_c(x = 0, y = 0, z = 0) = \int_{E_\gamma} \mathcal{L}(E_\gamma) dE_\gamma \quad .$$

where the co-ordinates of the decay have been included to remind us that we are considering a special case. Equation III.3.2 is based upon the intersection of two confocal circular cones (the collimator cone and the second γ-ray cone). If the decay does not occur on the axis of the collimators then the collimator cones are no longer circular but rather elliptic cones. For small deviations from the collimator axis however the cones may be considered to be approximately circular and the equation applied. In this case we expect that the probability will be reduced by a factor of $\simeq \cos\alpha \times \cos\beta$ (figure III.3.2) and

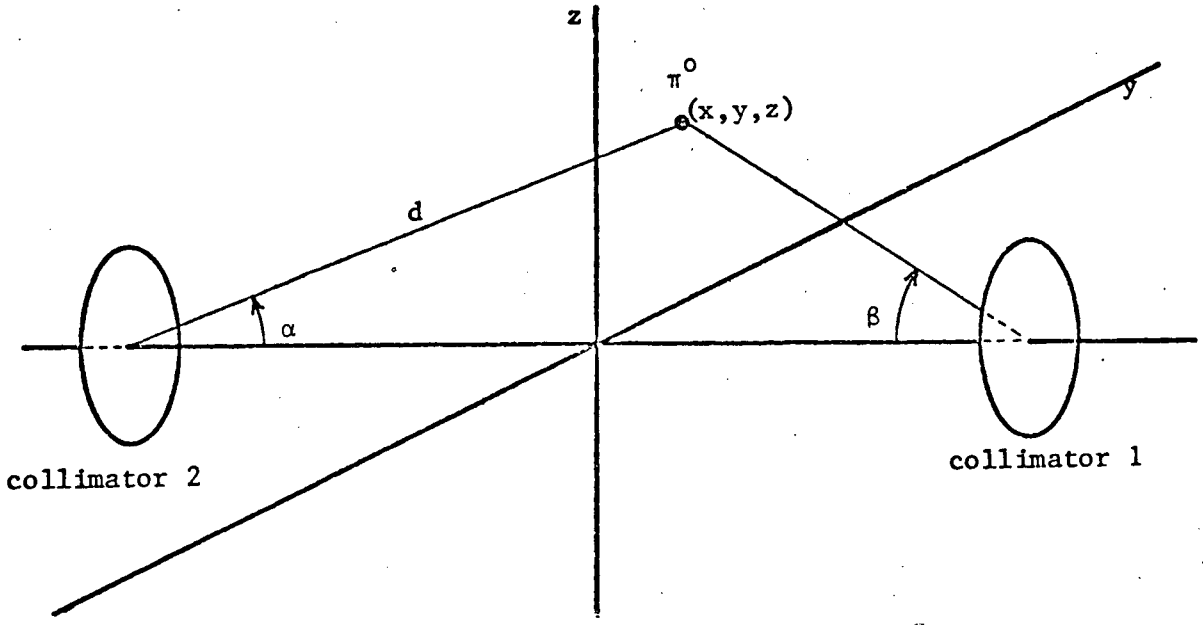

Figure III.3.2 π^o Decay off the Collimator Axis

we can apply this factor as a correction. In the present case the maximum deviation that we need consider is determined by the size of the target flask and was $\simeq 6^o$. Hence the error that we make in considering off axis points is less than 1%. The total coincidence efficiency for the target then is

$$\xi_c = \int_v \xi_c(x,y,z)\frac{dN\pi^-}{dV}\,dV \qquad \text{(III.3.4)}$$

where $\frac{dN\pi^-}{dV}$ is the density of stopped π^- at the target position (x,y,z). In the case of the deuterium coincidence efficiency equation (III.3.4) is seen to be effectively a 7-fold integration. In the case of the hydrogen coincidence efficiency the integration over the π^o energy spectrum is trivial however we still have a 6-fold numerical integration to perform. In order to make the calculation economical the functions $\xi_c(\alpha,d = 0)$

and $\xi_c(\alpha = 0,d)$ were evaluated at several values of α and d (where α and d are the angular deviation and decay collimator distance pictured in figure III.3.2; note that because of the symmetry around the collimator axis we may express $\xi_c(x,y,z)$ as $\xi_c(\alpha,d)$). These functions are shown plotted in figure III.3.3 and III.3.4. The functions $\xi_c(\alpha = 0,d)$ are well approximated by straight lines in this region of d. In fact $\xi_c(\alpha = 0,d)$ will have a maximum value when the solid angles of the two collimators are equal. This corresponds to a target position 10.4 cm. closer to MINA than was used in the present case, and we see that the function is indeed rising for positions closer to MINA. We assumed that this relationship would also be valid for small values of $\alpha \neq 0$ and hence

$$\xi(\alpha,d) = \frac{\xi(\alpha,0)\ \xi(0,d)}{\xi(0,0)}$$

The function $\xi(\alpha = 0,d)$ was evaluated from the straight line fit to the points plotted in figure III.3.3. The function $\xi(\alpha,d = 0)$ was obtained by means of linear interpolation between the data points plotted in figure III.3.4.

The π^- stopping distribution, $\frac{dN\pi^-}{dV}$ was presumed to be a function of 'y' only (the beam direction). It was taken to be a Gaussian distribution whose centroid was determined by the range of 51 MeV π^- in the scintillators, degrader, vacuum jacket, target windows and target liquid (ME74). The width of the Gaussian was determined by assuming that 49% of the "stopped pions" actually stop in the target liquid. The resulting distribution is shown in figure III.3.5. The fact that this estimate for the stopping distribution is very crude need not be of great concern as it will be shown that the shape of the stopping

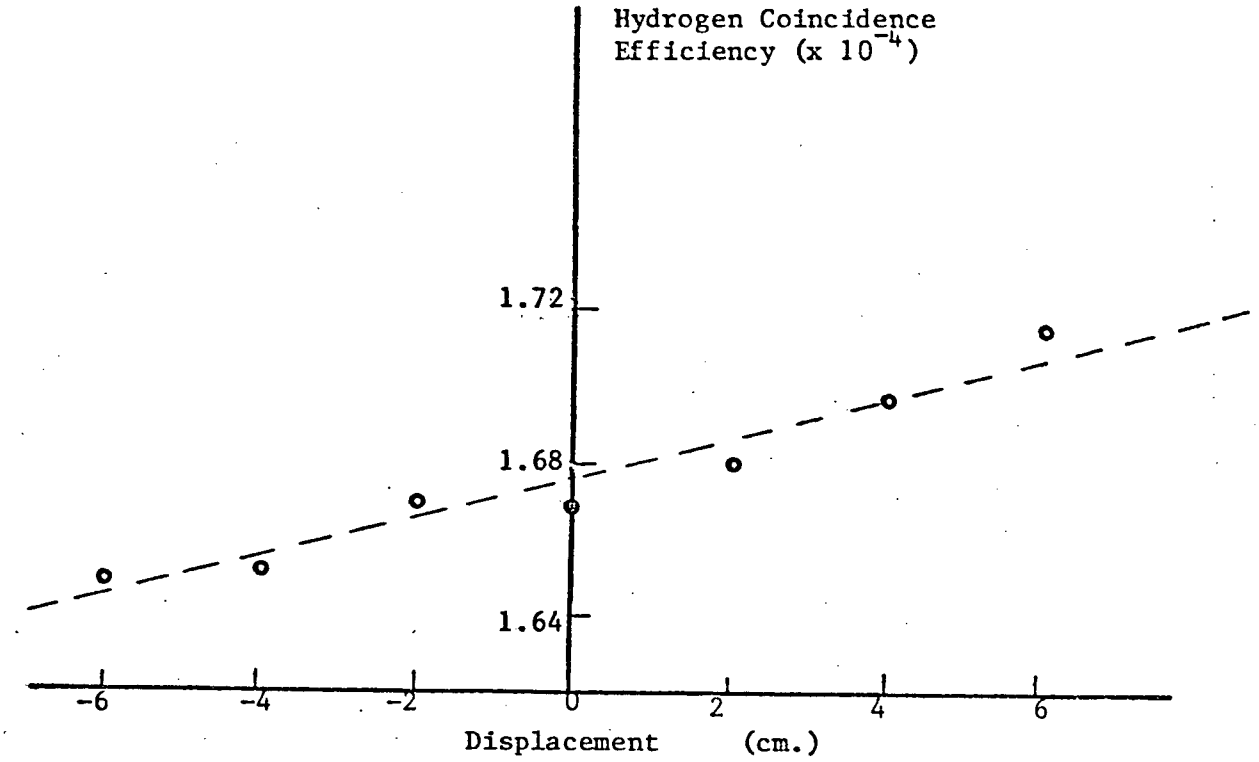

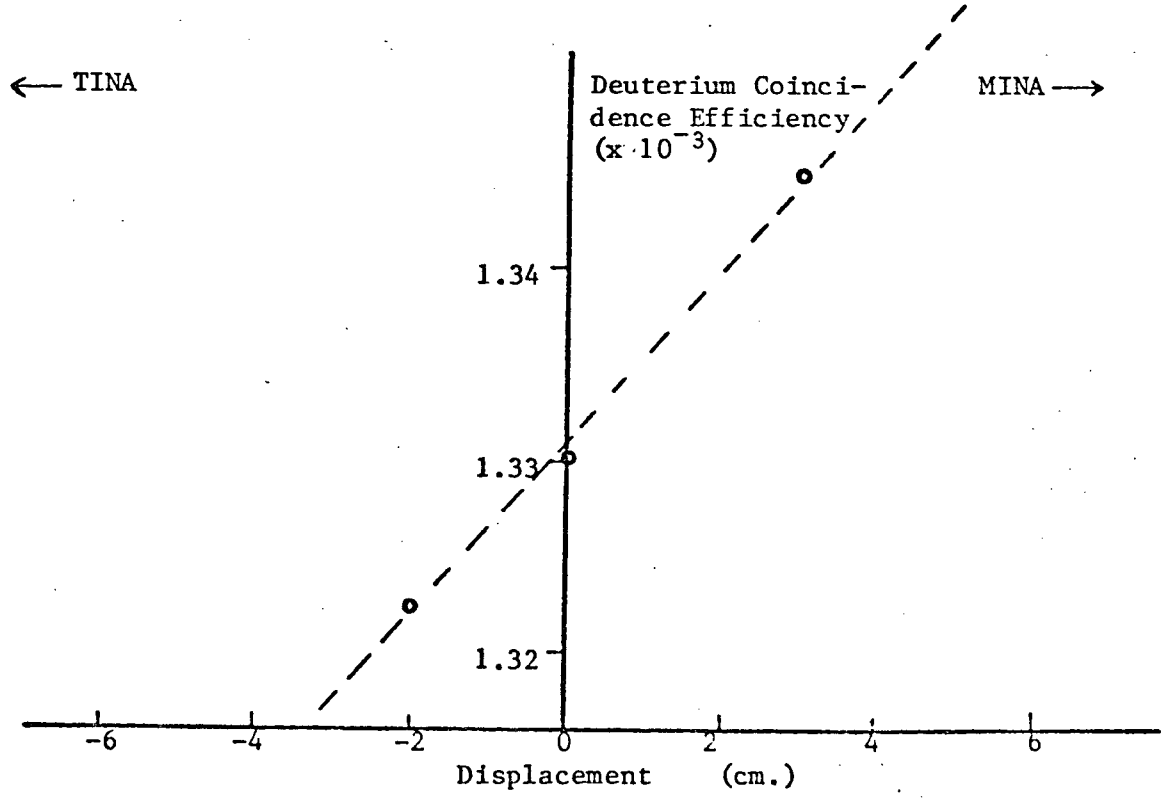

Figure III.3.3 Coincidence Efficiency as a function of displacement along collimator axis

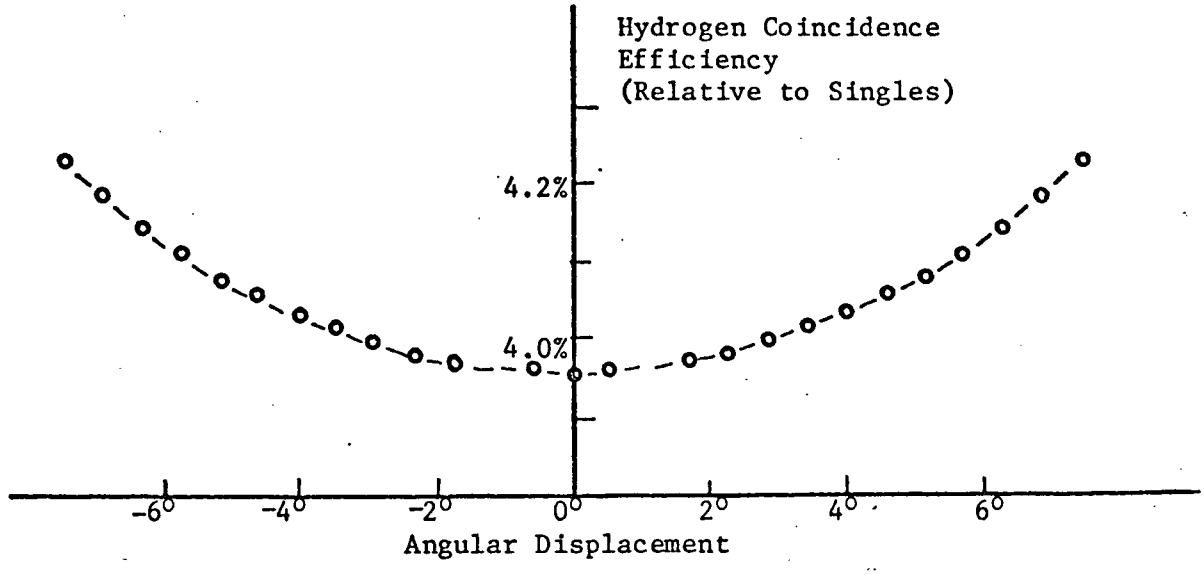

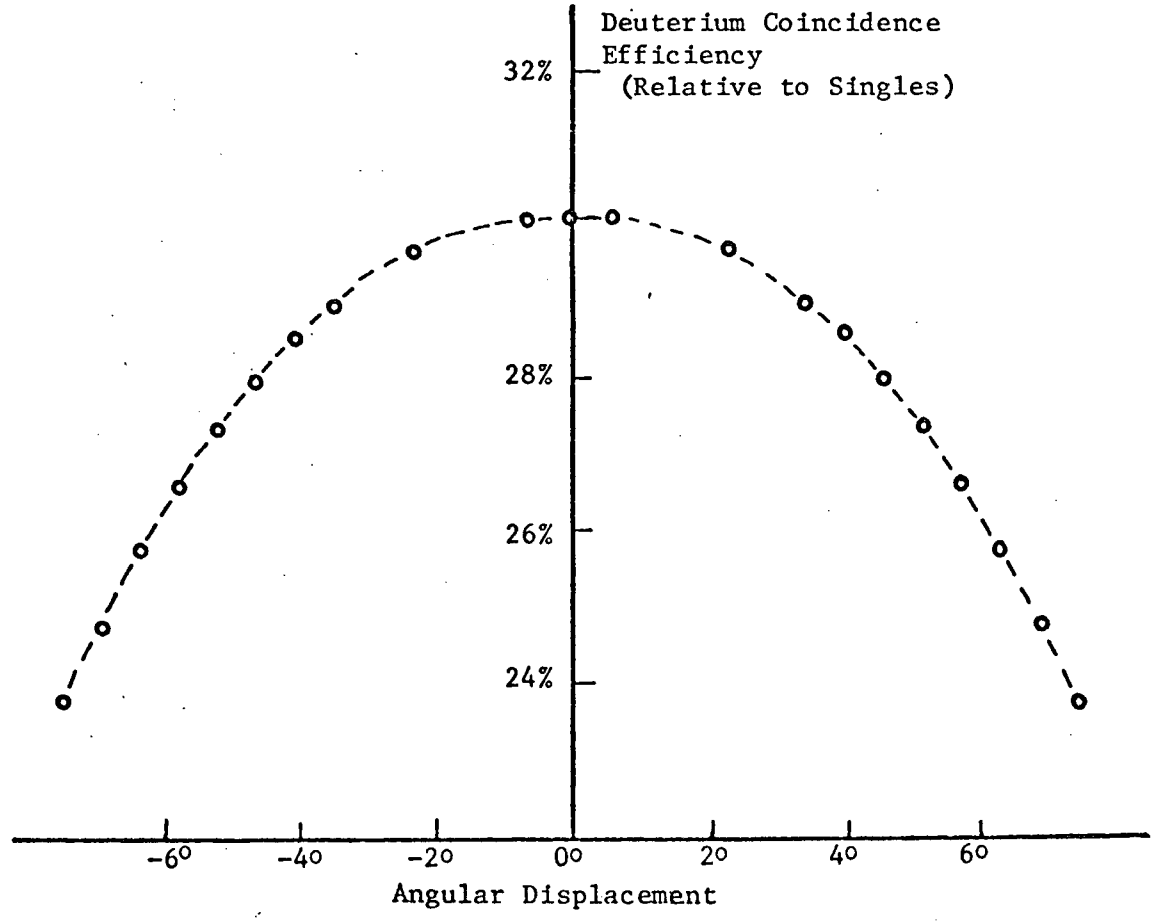

Figure III.3.4 Coincidence Efficiency as a function of angular displacement from collimator axis

distribution (at least for wide distributions) has little effect on the total efficiency. The chosen distribution serves the purpose of this demonstration.

The only remaining consideration in evaluating equation (III.3.3) to determine the total efficiency is the volume of integration to be used. Again, we found that we could tolerate a rather crude description of the active volume since the total efficiency was rather insensitive to this consideration.

The volume of integration is that volume of the target which is also in the volume of the π^- beam as defined by the counter 'C_2'. The beam divergence is primarily due to multiple scattering in the degrader and is well represented by a Gaussian distribution with a 6^o standard deviation (SP77). For the purpose of this calculation the beam was considered to uniformly fill a cone of 6^o half-angle. The radius of this cone exceeded the target radius at approximately the collimator axis. The error in the calculated efficiency due to the estimate of the beam volume was determined by considering the two extreme cases of a cylindrical beam volume the size of C_2 and a fully illuminated target volume. The errors in the efficiency calculation are summarized in the following table. The error due to finite binning in the numerical integration is large in the case of deuterium because of the integration over the pion energy distribution. In general the larger errors in the deuterium calculation are due to the more extreme variation of the function $\xi_c(\alpha,d)$ with α. The error due to the stopping distribution was determined by considering the difference in efficiency using the Gaussian distribution for $\frac{dN\pi}{dV}$ and using a constant stopping distribution. The values determined for the coincidence efficiencies are

$$\xi_{\pi H} = (1.74 \pm 0.026) \times 10^{-4}$$

$$\xi_{\pi D} = (1.166 \pm 0.042) \times 10^{-3}.$$

The coincidence lineshapes (equation (III.3.3)) have also been evaluated for deuterium and hydrogen. In the case of hydrogen the integration over the target volume has been performed. In the case of deuterium the lineshape is for a π^0 decay at the centre of the target. These lineshapes have been plotted in figure II.1.5.

ERROR IN EFFICIENCY CALCULATION DUE TO:	DEUTERIUM EFFICIENCY	HYDROGEN EFFICIENCY
1. Numerical Integration	2.2%	0.1%
2. Non-circular intersection of cones	0.5%	0.5%
3. Interpolation of $\xi(\alpha,d)$	1.5%	1.0%
4. Beam volume	1.7%	0.9%
5. Target length	1.6%	0.3%
6. Stopping distribution	0.7%	0.1%
TOTAL ERRORS	3.6%	1.5%

4. Corrections for In-Flight Interactions

The probability that a π^- which enters the target with kinetic energy T_o will interact in flight in a volume element Adx at position x in the target (figure III.4.1) is given by

$$dP_I(T_o,x) = \rho\sigma(T)dx \ ,$$

where ρ is the density of deuterium atoms in the target and $\sigma(T) = \sigma(T(x))$ is the cross section for the interaction.

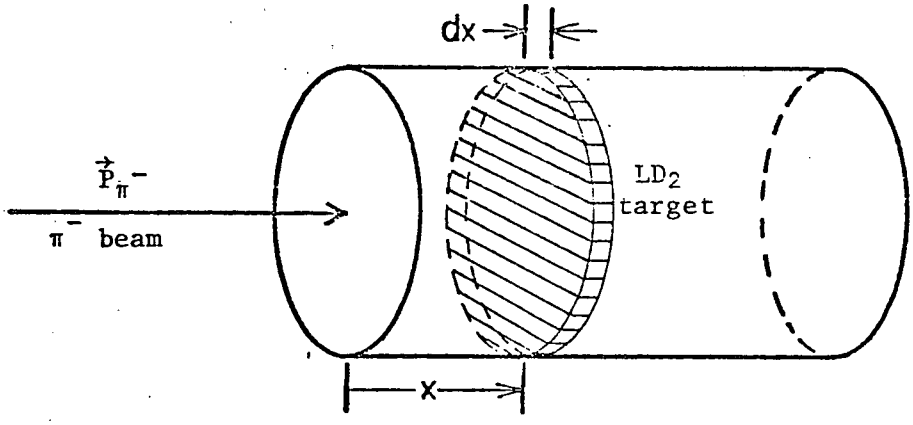

Figure III.4.1 Liquid Deuterium Target

The probability for observing the interaction is

$$dP_o(T_o,x) = \rho\sigma(T)\xi(T,x)dx$$

and the total probability for observing an interaction while in flight is

$$P_o(T_o) = \int_{x=0}^{x_r} \rho\sigma(T)\xi(T,x)dx \qquad \text{(III.4.1)}$$

where x_r is the range of the pion in the target. To determine the function T(x) we note that for pions of kinetic energy less than ≈50 MeV the stopping power in deuterium (ME74, TR76) is approximated to about 10% by

$$-\frac{dT}{dx} = aT^{-b} \qquad \text{(III.4.2)}$$

With T measured in MeV

$a = 10.87$

$b = 0.805.$

Integrating equation (III.4.2) gives

$$T(x) = (T_o^c - kx)^{1/c}$$

where c = 1.805 and k = 19.63. Then

$$x_r = \frac{T_o^c}{k}$$

A. Charge Exchange

In appendix III it is shown that for small energies

$$\sigma(T) = d\,\frac{(T+Q)^4}{\sqrt{T}} \qquad \text{(III.4.3)}$$

The constant 'd' was determined from the data of Rogers and Lederman (RO57) at 85 MeV. For T and Q measured in MeV

$$d = 2.05 \times 10^{-6}\text{mb} .$$

The function $\xi_c(T)$ has been evaluated at energies T = 0.0 MeV, 8.9 MeV and 18.9 MeV. It is found that this data fits the function

$$\xi_c(T) = \frac{33.12}{T+Q} \qquad \text{(III.4.4)}$$

to better than 10%. Substituting (III.4.2), (III.4.3) and (III.4.4) into (III.4.1) and performing the integration gives

$$P_o(T_o) = 1.56 \times 10^{-15} T_o^{4.305} \left\{1.0 + 3.92\left(\frac{Q}{T_o}\right) + 5.60\left(\frac{Q}{T_o}\right)^2 + 3.31\left(\frac{Q}{T}\right)^3\right\} \qquad \text{(III.4.5)}$$

To make use of this relationship we must know the distribution of the pion kinetic energies at the face of the target. We took the original momentum distribution to be Gaussian with a centroid at 130 MeV/c and a FWHM of 15%. (The M9 momentum byte has been measured at T_{π^-} = 30 MeV for a 10 cm. Be target and 10 cm. horizontal slits as 15% FWHM (BR76)).

This momentum distribution was divided into equal bins and for each bin the energy at the target face and the number of in-flight charge exchange γ-rays expected from the bin were determined. The momentum distribution and the expected number of in-flight charge exchange γ-rays for each bin are plotted in figure III.4.2. Also shown on the abscissa are the target entry energies for the given momentum bin. There are a total of 17.2 coincidence γ-rays expected from charge exchange in flight. We have used equation (III.4.5) to estimate that of these only 1.7 coincidence γ-rays occur from in flight interactions below 18.9 MeV. A charge exchange coincidence γ-ray lineshape for 18.9 MeV incident π^- has been calculated using the methods outlined in the previous section and is plotted in figure III.4.3. Lineshapes for higher energy interactions will have an even larger energy spread and a greater dip in the central region. Thus the use of the 18.9 MeV lineshape to estimate the contribution from in flight events under the hydrogen and deuterium peaks is expected to give a result that is somewhat too large. The contribution under the hydrogen peaks is expected to be less than 7.8 γ-ray events. The contribution under the deuterium data is expected to be less than 2.0 γ-ray events.

It is realized that many of the approximations used to arrive at these figures are rather crude. For example, the stopping power, as given by equation (III.4.2) is expected to be good to only about 10% in the 30-50 MeV region and it is this energy region which largely determines the in-flight contribution. Furthermore the extrapolation of the low energy cross section relationship (equation III.4.3) to energies as large as 85 MeV is questionable. Despite these shortcomings the calculation does point out that the in flight charge exchange contribution

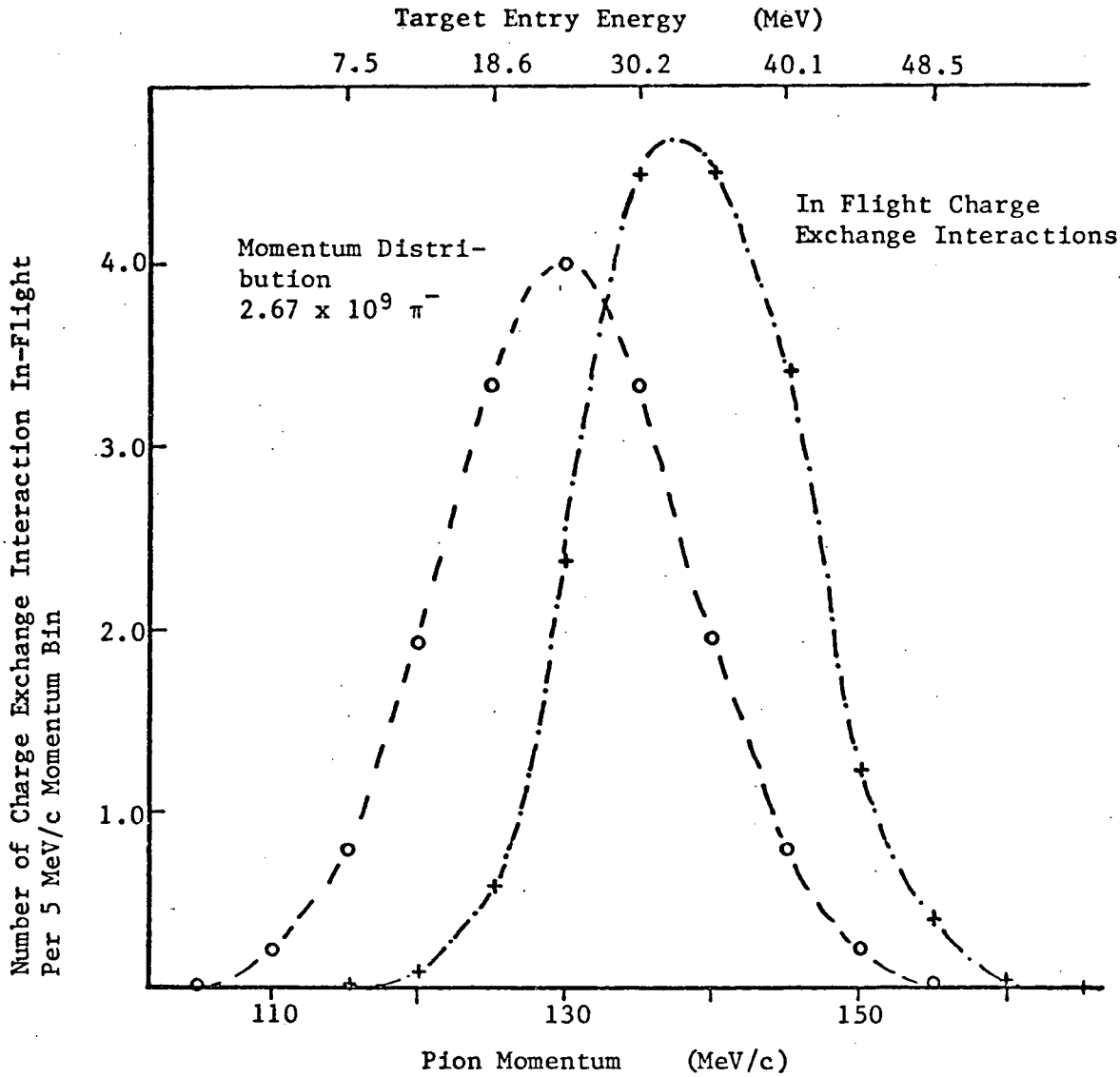

Figure III.4.2 π^- Momentum Byte and In flight Charge Exchange

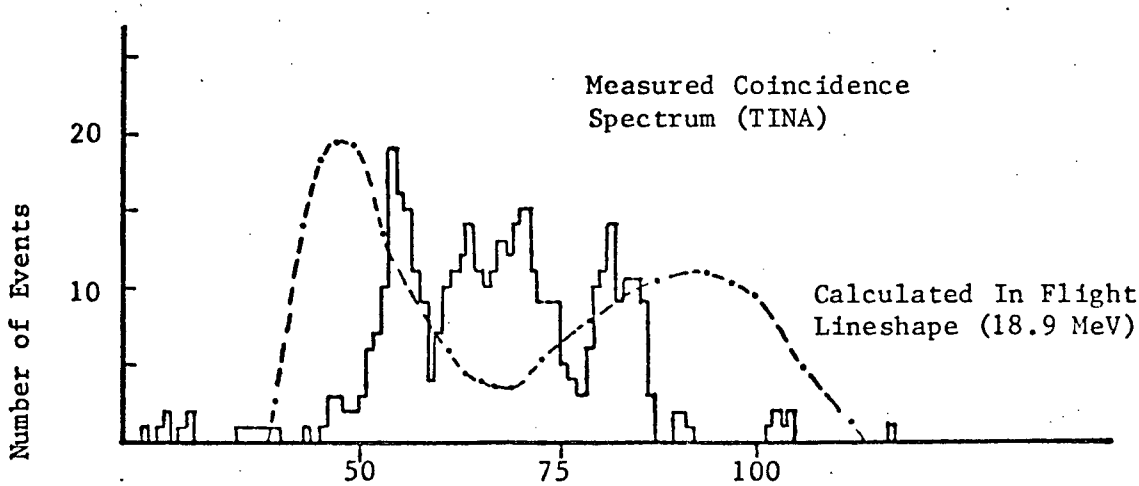

Figure III.4.3 Calculated Lineshape for 18.9 MeV π^-

is dominated by π^- energies greater than 18.9 MeV. Thus, on the basis of figure III.4.3, we would expect about 30% of the in flight charge exchange coincidence γ-rays to have energies above the high energy hydrogen coincidence peak. The previous calculation suggests that we should find 5 γ-ray events in this region. In fact we see 11 events. This discrepancy may be interpreted either as an indication that our calculation is low by a factor of two or that the 18.9 MeV lineshape is not a good description of the "average" lineshape for the energy region above 18.9 MeV. The former interpretation will increase our corrections by a factor of two; the latter could decrease them considerably. The correct interpretation of course is some combination of these two. (It is clear that the 18.9 MeV lineshape has too little weight in the region above the high energy hydrogen coincidence peak. However the actual lineshape can not have more than 50% of its area in this region, so this alone can not account for the discrepancy). In any case the size of the correction is less than the error in the number of events in either the hydrogen or the deuterium coincidence spectrum and so it is expedient to avoid these uncertainties simply by applying large error limits to the corrections. These are taken as 2.0 ± 2.0 in the case of the correction to the deuterium coincidence counts and 7.8 ± 7.8 in the case of the correction to the hydrogen coincidence counts.

B. Radiative Capture

The determination of the correction due to in flight radiative capture is more straight forward. We again make use of equation (III.4.1) to determine the probability of observation. In this case however the efficiency is just the singles efficiency and is not a function of energy. Furthermore, the cross-section now is given by

$$\sigma(T) = a\frac{(T + Q)^2}{\sqrt{T}}$$

and in this case Q = 136 MeV. The effect of this is a rather slow variation of the cross section with energy in the range of interest. Again 'a' was taken from the data at 85 MeV where the cross section is 1.1 ± 0.6 mb (RO57). Since the cross section is rising for energies below 40 MeV care was taken to avoid integrating beyond the end of the target. The net result of the calculation was an expected contribution of 8100 ± 4400 radiative capture events from π^- in flight. This represents a 1% correction to the total number of radiative capture events.

5. The Final Analysis

The following table (Table III.5.1) summarizes the measured and calculated quantities which were used to determine the charge exchange branching ratio from our data. Using the ratio of the charge exchange rate to the radiative capture rate (equation III.2.1)) we find

$$R_1 = \frac{D_\pi}{\xi_{\pi D}} \frac{\xi_S}{N_\gamma (\pi^- d \to \gamma nn)} \frac{1}{S+1} = (1.46 \pm 0.19) \times 10^{-4}$$

Using the ratio of the charge exchange rate in hydrogen to the charge exchange rate in deuterium (equation (III.2.2)) we find

$$R_2 = R_H C_H \frac{D_\pi}{\xi_{\pi D}} \frac{\xi_{\pi H}}{H_\pi} = (1.16 \pm 0.33) \times 10^{-4}$$

In determining the errors assigned to this second number it was necessary to consider the negative correlation between the errors in D_π and H_π and between the errors in $\xi_{\pi H}$ and $\xi_{\pi D}$. The correlation in the D_π and H_π terms arises because the sum of the two terms is constrained. The correlation in the $\xi_{\pi H}$ and $\xi_{\pi D}$ terms is a result of the opposite curvatures of the functions $\xi_{\pi H}(\alpha)$ and $\xi_{\pi D}(\alpha)$ (figure III.3.4). Furthermore it is not legitimate to simply consider the weighted mean of the two numbers as an average value because the two numbers are not independent. To obtain a properly weighted average value we must separate the common terms and not consider them in the weighting. In detail

TABLE III.5.1 - Summary of Data

D_π = 166.0 ± 20.0 Number of Deuterium Coincidence Events. Corrected for in-flight charge exchange.

H_π = 187.8 ± 17.4 Number of Hydrogen Coincidence Events. Corrected for in-flight charge exchange.

$N_\gamma(\pi^- d \rightarrow \gamma nn)$ = 806122 ± 8000 Number of Deuterium Radiative Capture Events. Corrected for in-flight radiative capture, contributions from deuterium and hydrogen charge exchange and hydrogen radiative capture.

C_H = $(1.45 \pm 0.29) \times 10^{-3}$ Effective concentration of hydrogen.

ξ_s = $(3.29 \pm 0.03) \times 10^{-3}$ TINA singles γ-ray efficiency.

$\xi_{\pi D}$ = $(1.166 \pm 0.042) \times 10^{-3}$ Efficiency for observing deuterium charge exchange γ-rays.

$\xi_{\pi H}$ = $(1.740 \pm 0.026) \times 10^{-4}$ Efficiency for observing hydrogen charge exchange γ-rays.

S = 2.97 ± 0.17 Ratio of π^- absorption and radiative capture rates in deuterium (world average (excluding CH54)).

R_H = 0.607 ± 0.002 Charge Exchange branching ratio in hydrogen (Most recent result (SP77)).

$$\overline{R} = \frac{D_\pi}{\xi_{\pi D}} \left\{ \frac{1}{W_1 + W_2} W_1 \left(\frac{\xi s}{N_\gamma(\pi^- d \to \gamma nn)} \right) \frac{1}{S+1} + W_2 R_H C_H \frac{\xi_{\pi H}}{H_\pi} \right\}$$

or

$$\overline{R} = \frac{D_\pi}{\xi_{\pi D}} \frac{1}{W_1 + W_2} (W_1 F_1 + W_2 F_2)$$

where

$$F_1 = \frac{\xi s}{N_\gamma(\pi^- d \to \gamma nn)} \frac{1}{S+1}$$

$$F_2 = R_H C_H \frac{\xi_{\pi H}}{H_\pi}$$

and the weighting factors W_1 and W_2 are assigned in the usual fashion. That is

$$W_1 = \frac{1}{dF_1^2} \text{ and } W_2 = \frac{1}{dF_2^2} .$$

When written in this format it is clear that the relatively large errors in C_H and H_π will result in the second method being weighted very lightly compared with the first. In fact the average value, which I quote as the final result is

$$R = 1.45 \times 10^{-4} \pm 0.19 \times 10^{-4} .$$

From this we determine

$$K = 5.76 \times 10^{-4} \pm 0.71 \times 10^{-4}$$

where the relative error is slightly decreased because the value of 'S' is eliminated from the calculation.

CHAPTER IV

DISCUSSION

1. The Charge Exchange Branching Ratio

The branching ratio for pion charge exchange in deuterium ties in with other low energy pion results. In particular, in a recent calculation Beder (MA77) has used the impulse approximation to relate the charge exchange rate in deuterium to the hydrogen charge exchange scattering length. In a recent analysis of $\pi^+ d \to pp$ cross section data Spuller (SP75) presents a figure which demonstrates the relationships between the low energy pion data. This is shown in figure IV.1.1 with the relationship of the deuterium charge exchange rate included.

Following Beder's calculation (BE76, MA77) we note that the capture rate to a final state $|f\rangle$ from an initial state $|i\rangle$ is given in terms of the $|i\rangle \to |f\rangle$ S-matrix as

$$\omega(f) = \int d\rho_f \left[(2\pi)^4 \delta^4(p_f - P_i)\right]^{-1} |\langle f|S|i\rangle|^2 \qquad \text{(IV.1.1)}$$

where $d\rho_f$ is the density of final states and P_f and P_i are the final and initial four-momenta. We may expand the S-matrix element in terms of a complete set of $\pi^- d$ plane wave states. In the $\pi^- d$ rest frame

$$\langle f|S|i\rangle \sim \int \langle f|S|\pi(\vec{q})d(-\vec{q})\rangle\langle\pi(\vec{q})d(-\vec{q})|i(\text{atomic})\rangle d^3q$$

where $\vec{q}$ is the π^- momentum. We recognize the second term as the Fourier transform of the initial atomic wave function in $\vec{r}$ space. This transform

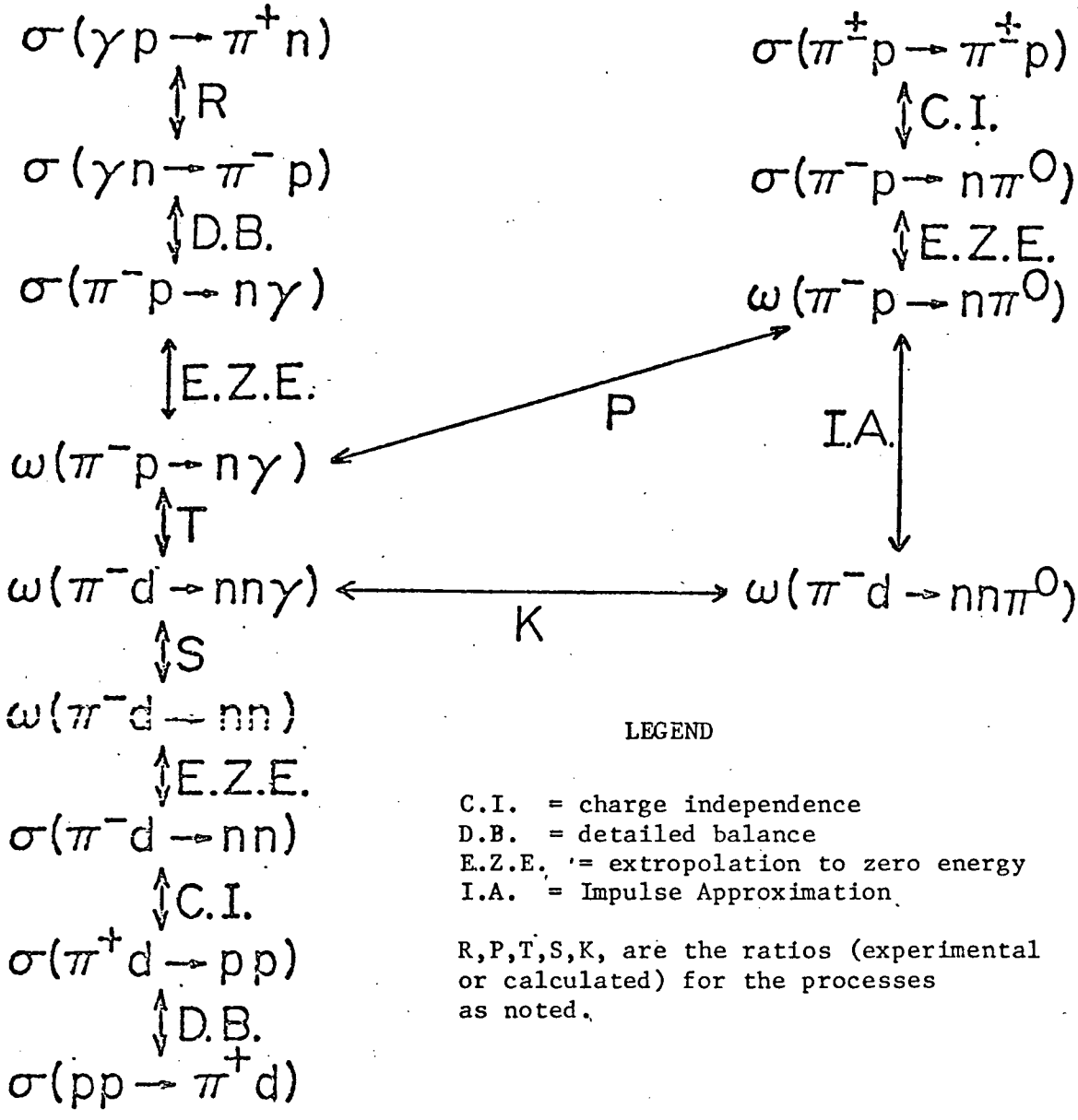

Figure IV.1.1 Relations Between Low Energy Pion Reactions

is negligible for $|\vec{q}| >> \frac{1}{a_\pi}$ where in the present case, a_π is the π^- Bohr radius. The first term is the conjugate fourier transform of a function in $\vec{r}$ space which has a range of approximately the nuclear potential and hence will be nearly constant over the short range ($\vec{q} \approx 0$) of the second term. Thus we may simplify expression IV.1.1 by removing the first term from the integral.

$$<f|S|i> \sim <f|S|\pi(0)d(0)> \int <\pi^-(\vec{q})d(-\vec{q})|i(\text{atomic})>d^3q$$

Using this approximation in equation IV.1.1 gives

$$\omega \sim \int d\rho_f \left[(2\pi)^4\delta^4(P_f - P_i)\right]^{-1} |<f|S|\pi(0)d(0)>|^2 \left[\int <\pi^-(\vec{q})d(-\vec{q})|i(\text{atomic})>d^3q\right]^2$$

$$= \lim_{q\to 0} q\sigma(\pi^-d \to f) \left(\int <\pi^-(\vec{q})d(-\vec{q})|i(\text{atomic})>d^3q\right)^2$$

where σ is the free particle cross-section (without coulomb effects) for initial plane wave π^-d states to interact. All of the details of the initial atomic state are wrapped up in the integral. Since we are considering the ratio of transition rates to different final states the effects of the coulomb distortion of the initial atomic state do not enter. In particular

$$\frac{\omega(\pi^-d \to \pi^0 nn)}{\omega(\pi^-d \to nn)} = \frac{\lim_{q\to 0} q\sigma(\pi^-d \to \pi^0 nn)}{\lim_{q\to 0} q\sigma(\pi^-d \to nn)} . \qquad \text{(IV.1.2)}$$

The charge exchange cross-section may be expressed in terms of the S-matrix.

$$q\sigma(\pi^- d \to \pi^0 nn) =$$

$$\int \frac{d^3q' d^3k_1 d^3k_2}{(2\pi)^9} \left[(2\pi)^4 \delta^4(P_f - P_i)\right]^{-1} 1/3 \sum_{\text{spins}} |\langle \pi^0 nn|S|\pi^- d\rangle|^2 \cdot \tfrac{1}{2} \qquad \text{(IV.1.3)}$$

where q', k_1, k_2 are the final π^0 and two neutron momenta respectively. The S-matrix is anti-symmetrized in k_1 and k_2. The capture from the initial state is s wave so parity conservation and angular momentum conservation results in a triplet spin state for the final nucleons. Since we do not look at spin here $1/3 \sum_{\text{spins}} |S|^2$ is equivalent to $|S|^2$ ignoring spins. The final factor of $\tfrac{1}{2}$ avoids double counting the identical nucleons. We now define a reduced scattering matrix $\bar{S}$ by explicitly including the energy conservation delta function; viz.

$$\langle f|\bar{S}|i\rangle = \left[2\pi\delta(E_f - E_i)\right]^{-1} \langle f|S|i\rangle.$$

We expand the reduced matrix element in terms of a complete set of n and p plane wave states.

$$\langle \pi^0 nn|\bar{S}|\pi^- d\rangle = (2\pi)^{-6} \int d^3t d^3s \, \langle \pi^0 k_2 k_1|\bar{S}|\pi^- n(\vec{t}) p(\vec{s})\rangle \langle n(t) p(\vec{s})|d\rangle$$

$$- \langle \pi^0 k_2 k_1|\bar{S}|\pi^- n(\vec{t}) p(\vec{s})\rangle \langle n(\vec{t}) p(\vec{s})|d\rangle$$

In the impulse approximation the initial neutron takes only a spectator role. Hence

$$\langle \pi^0 n(\vec{k}_1) n(\vec{k}_2)|\bar{S}|\pi^- n(\vec{t}) p(\vec{s})\rangle = (2\pi)^3 \delta^3(\vec{k}_1 - \vec{t}) \langle \pi^0 n(\vec{k}_2)|\bar{S}_{\pi N}|\pi^- p(\vec{s})\rangle$$

$$= \frac{(2\pi)^3 \delta^3(\vec{k}_1 - \vec{t}) \, \delta^3(\vec{q}' + \vec{k} - \vec{q} - \vec{s}) \, 8\pi \, W_{\pi N} \, f(\pi^- p \to \pi^0 n)}{\left\{2E(\pi^0) \cdot 2E_n(\vec{k}_2) \cdot 2E(\pi^-) \cdot 2E_p(\vec{s})\right\}^{\frac{1}{2}}}$$

where $\vec{t}$ and $\vec{s}$ are the momenta of the neutron and proton plane wave states, $W_{\pi N}$ is the total energy in the pion-nucleon center of mass and $f(\pi^- p \to \pi^0 n)$ is the hydrogen charge-exchange scattering amplitude. In the limit $q \to 0$ $W_{\pi N} = M + \mu$ (the sum of the nucleon and pion masses) and $f(\pi^- p \to \pi^0 n)$ is replaced by the hydrogen charge exchange scattering length, $a(\pi^- p \to \pi^0 n)$. With these considerations we determine from equation (IV.1.3) that

$$\lim_{q \to 0} q\sigma(\pi^- d \to \pi^0 nn)$$

$$= \frac{96\pi (M + \mu)^2}{\mu M} \; a^2(\pi^- p \to \pi^0 n) \int dq' k(q') q'^{-2} \left| F(q') \right|^2 \qquad \text{(IV.1.4)}$$

where $F(q) = \int j_1(kr) j_1\left(\frac{qr}{2}\right) \phi_d(r) r^2 dr,$

$$k = \left\{ M\left(Q - \frac{q'^2}{2\bar{\mu}}\right) \right\}^{\frac{1}{2}},$$

Q = reaction Q-value (1.1 MeV),

$\bar{\mu}$ = neutral pion reduced mass,

ϕ_d = unit normalized deuteron wave function.

$$= \left(\frac{\alpha\beta(\alpha + \beta)}{2\pi(\alpha - \beta)^2} \right)^{\frac{1}{2}} \frac{e^{-\alpha r} - e^{-\beta r}}{r}$$

$\alpha^{-1} = 4.3$ fm

$\beta = 7\alpha$

A correction may be made for double scattering. This is of order

$$\left\{a(\pi^- n \to \pi^- n) + a(\pi^0 n \to \pi^0 n)\right\} a(\pi^- p \to \pi^0 n) \langle \phi_{nn} (1 = 1) \left| \frac{1}{r_{np}} \right| \phi_d \rangle$$

and contributes a -1% correction to the impulse approximation amplitude. Using the most recent result for the hydrogen charge exchange scattering length ($a(\pi^- p \to \pi^0 n) = 0.175$ fm (NA76)) in equation (IV.1.4) we find

$$\lim_{q \to 0} q\sigma(\pi^- d \to \pi^0 nn) = 0.0358 \text{ MeV mb} \qquad \text{(IV.1.5)}$$

The denominator of equation (IV.1.2) is evaluated by assuming that for Coulomb corrected cross-sections $\sigma(\pi^- d \to nn) = \sigma(\pi^+ d \to pp)$. The threshold behavior of the latter cross-section has been analysed in detail by Spuller and Measday (SP75) who fit Coulomb corrected data to a function of the form

$$\sigma(\pi^+ d \to pp) = \frac{2}{3} \frac{P_p^2}{\eta^2} \left\{\alpha\eta + O(\eta^2)\right\}$$

where P_p is the proton center of mass momentum in units of $M_\pi c$, α is a fitting parameter and $\eta = q/\mu$. They find the preferred range for α to be

$$0.25 \text{ mb} \leq \alpha \leq 0.29 \text{ mb}.$$

In the limit that $q \to 0$ this corresponds to

$$162 \text{ MeV} \cdot \text{mb} \leq \lim_{q \to 0} q\sigma(\pi^- d \to nn) \leq 187 \text{ MeV mb}. \qquad \text{(IV.1.6)}$$

The charge exchange branching ratio is given by

$$R = \frac{\omega(\pi^- d \to \pi^0 nn)}{\omega(\pi^- d \to nn)} \cdot \frac{\omega(\pi^- d \to nn)}{\omega(\pi^- d \to all)} .$$

The first factor is determined by equation (IV.1.2) and the subsequent results (IV.1.5) and (IV.1.6). The second factor is determined from empirical value for S (2.97 ± 0.17). Thus the theoretical calculation predicts a branching ratio

$$1.39 \times 10^{-4} \leq R \leq 1.59 \times 10^{-4}$$

which is in good agreement with our experimental value

$$R = (1.45 \pm 0.19) \times 10^{-4} .$$

It should be pointed out that using the earlier 'recommended' value of Pilkuhn et al (PI73) for the hydrogen charge exchange scattering length ($a(\pi^- p \to \pi^0 n) = 0.193 \pm 0.013$ fm) results in a branching ratio

$$1.67 \times 10^{-9} \leq R \leq 1.91 \times 10^{-4}$$

in distinct conflict with the present value.

LIST OF REFERENCES

BE76 D. Beder, Private Communication

BE77 D. Beder, Private Communication

BI76 J.A. Bisterlich, S. Cooper, K.M. Crowe, F.T. Shively, E.R. Grilly, J.P. Perroud, R.H. Sherman, H.W. Baer, P. Truol, Phys. Rev. Lett. 36, 942 (1976)

BR51 K. Brueckner, R. Serber, K. Watson, Phys. Rev. 81, 575 (1951)

BR76 D. Bryman, Triumf Internal Report, Feb 19, 1976

CH54 W. Chinowsky, J. Steinberger, Phys. Rev. 95, 1561 (1954)

CH55 W. Chinowsky, J. Steinberger, Phys. Rev. 100, 1476 (1955)

CO61 V.T. Cocconi, T. Tazzini, G. Fidecaro, M. Legros, N.H. Litman, A.W. Merrison, Nuovo Cimento 22, 494 (1961)

HA65 R.P. Haddock, R.M. Salter Jr., M. Zeller, J.B. Czirr, D.R. Nygren, Phys. Rev. Lett. 14, 318 (1965)

KL64 P.K. Kloeppel, Nuovo Cimento 34, 11 (1964)

KR68 Z.V. Krumshtein, V.I. Petrukhin, L.I. Ponomarev, Yu.D. Prokoshkin, Soviet Physics JETP 27, 906 (1968)

KU59 J.A. Kuehner, A.W. Merrison, S. Tornabene, Proc. Phys. Soc. (London) 73, 551 (1959)

LE62 M. Leon, H.A. Bethe, Phys. Rev. 127, 636 (1962)

MA77 R. MacDonald, D.S. Beder, D.C. Berghofer, M.D. Hasinoff, D.F. Measday, M. Salomon, J. Spuller, T. Suzuki, J.M. Poutissou, R. Poutissou, P. Depommier, J.K.P. Lee, Phys. Rev. Lett. (accepted for publication 1977)

MC64 M. McClintock, Cryogenics, Reinhold Pub. Corp., New York (1964)

ME74 D.F. Measday, M.N. Menard, J.E. Spuller, TRIUMF Kinematic Handbook

ME77 D.F. Measday, Private communication.

NA76 M.M. Nagels et al., Nucl. Phys. B109, 1 (1976)

PA51 W.E.H. Panofsky, R.L. Aamodt, J. Hadley, Phys. Rev. 81, 565 (1951)

PE64 V.I. Petrukin, Yu.D. Prokoshkin, Nuclear Physics 54, 414 (1964)

PE69 V.I. Petrukin, Yu.D. Prokoshkin and V.M. Suvorov, Sov. Phys. JETP 28, 1151 (1969)

PI73 H. Pilkuhn, W. Schmidt, A.D. Martin, C. Michael, F. Steiner, B.R. Martin, M.M. Nagels, J.J. de Swart, Nucl. Phys. B65, 460 (1973)

PO73 L.I. Ponomarev, Annual Reviews of Nuclear Science, 1973

RO57 K.C. Rogers, L.M. Lederman, Phys. Rev. 105, 247 (2957)

RY63 J.W. Ryan, Phys. Rev. 130, 1554 (1963)

SH68 L.I. Schiff, Quantum Mechanics, McGraw-Hill Book Co., New York (1968)

SP75 J. Spuller, D.F. Measday, Phys. Rev. D12, 3550 (1975)

SP77 J. Spuller 1.,3., Submitted to Physics Letters (1977)
2., Private communication

TA51 S. Tamor, Phys. Rev. 82, 38 (1951)

TR74 P. Truol, H.W. Baer, J.A. Bisterlich. K.M. Crowe, N. de Botton, J.A. Helland, Phys. Rev. Lett. 32, 1268 (1974)

TR76 T.G. Trippe et al., "Review of Particle Properties", Reviews of Mod. Phys. 48, no.2, part II (April 1976)

WA51 K.M. Watson, R.N. Stuart, Phys. Rev. 82, 738 (1951)

YA50 C.N. Yang, Phys. Rev. 77, 242 (1950)

ZA65 O.A. Zaimidoroga, M.M. Kulyukin, R.M. Subyaev, I.V. Falomkin, A.I. Filippov, V.M. Tsupko-Sitnikov, Yu.A. Shcherbakov, Soviet Physics JETP 21, 848 (1965)

APPENDIX I

NEUTRAL PION KINEMATICS

1. Gamma Ray Doppler Shift

The decay of the π^o in the lab frame is pictured in figure AI.1.1.

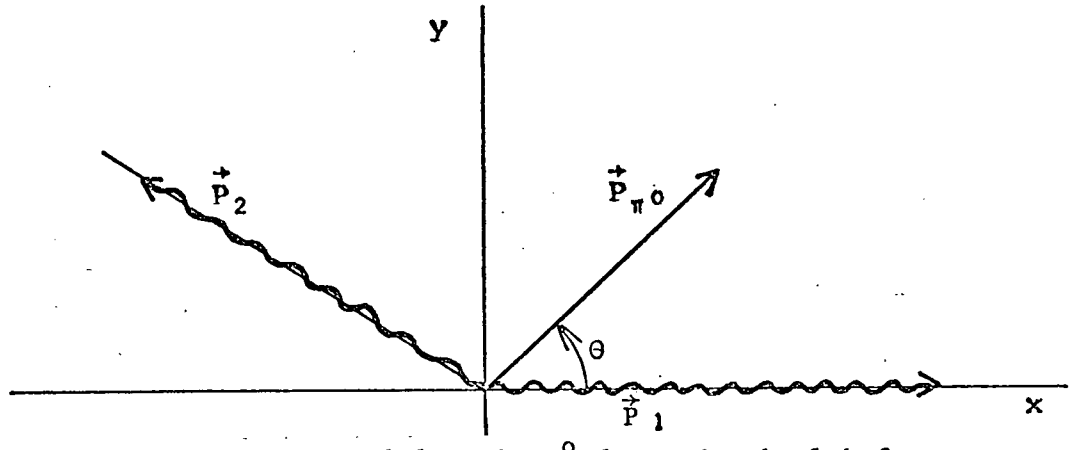

Figure AI.1.1 – The π^o decay in the lab frame

We choose the x axis to lie along the direction of one of the gamma rays with the origin at the position of the π^o decay.

The statements of conservation of energy and momentum are:

$$P_{2x} + P_{1x} = P_{\pi x} = P_\pi \cos\theta \tag{1}$$

$$P_{2y} = P_{\pi y} = P_\pi \sin\theta \tag{2}$$

$$P_{1x} + (P_{2x}^2 + P_{2y}^2)^{\frac{1}{2}} = (M_\pi^2 + P_\pi^2)^{\frac{1}{2}} \tag{3}$$

We square and add (1) and (2) to obtain

$$P_{2x}^2 + P_{1x}^2 + P_{2y}^2 + 2P_{1x}P_{2x} = P_\pi^2$$

and subtract this from the square of (3) to find

$$2P_{1x}((P_{2x}^2 + P_{2y}^2)^{\frac{1}{2}} - P_{2x}) = M_\pi^2$$

We now substitute from (1) and (3) for the components of P_2.

$$2P_{1x}((M_\pi^2 + P_\pi^2)^{\frac{1}{2}} - P_{1x} - P_\pi\cos\Theta + P_{1x}) = M_\pi^2$$

$$P_{1x} = \frac{1}{2}\frac{M_\pi^2}{(M_\pi^2 + P_\pi^2)^{\frac{1}{2}} - P_\pi\cos\Theta}$$

Now $P_{1x} = E_{\gamma 1}$ and $(M_\pi^2 + P_\pi^2)^{\frac{1}{2}} = E_\pi$. Hence

$$E_{\gamma 1} = \frac{1}{2}\frac{M_\pi^2}{E_\pi - P_\pi\cos\Theta}$$

2. The γ-spectrum Resulting from Isotropic π^0 Decay

Let dnγ be the number of γ-rays per unit pion solid angle in the lab frame

$$dn_\gamma = \frac{dN_\gamma}{d\Omega_\pi}$$

We first consider those pions whose momentum is contained in the elemental solid angle $d\Omega_\pi$. In the pion rest frame the γ-rays are isotropically distributed. Hence

$$dn_\gamma = k d\Omega_\gamma'$$

or

$$\frac{dn_\gamma}{d(\cos\theta')} = 2\pi k \qquad (1)$$

where the prime denotes the pion rest frame. In the lab frame this distribution is pushed forward in the direction of the pion momentum.

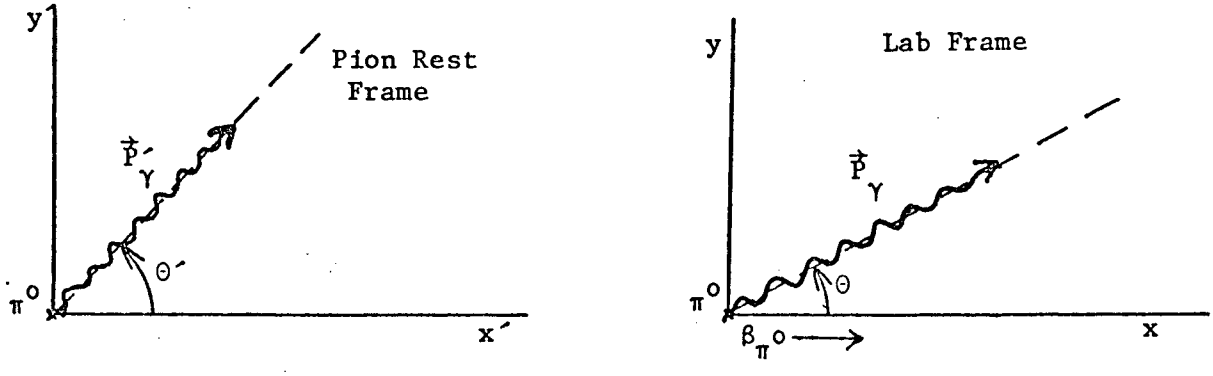

Figure AI.2.1 - Center of Mass - Lab transformations

The situation is depicted in figure AI.2.1. The pion rest frame is moving with velocity β_π with respect to the lab frame and $\beta'_{LAB} = -\beta_\pi$. For the γ-ray in the pion rest frame (with c = 1)

$$v'_x = \cos\Theta' \ .$$

In the lab frame

$$v_x = \cos\Theta \ .$$

The relativistic velocity addition equations connect these two velocities.

$$v_x = \frac{v'_x - \beta'_{LAB}}{1 - \beta'_{LAB} v_{x'}} \ .$$

Then

$$\cos\Theta = \frac{v_{x'} - \beta'_{LAB}}{1 - \beta'_{LAB} v_{x'}} = \frac{\cos\Theta' - \beta'_{LAB}}{1 - \beta'_{LAB}\cos\Theta'}$$

so

$$\cos\Theta = \frac{\cos\Theta' + \beta_\pi'}{1 + \beta_\pi \cos\Theta'}$$

and conversely

$$\cos\Theta' = \frac{\cos\Theta - \beta_\pi}{1 - .\beta_\pi \cos\Theta} \ . \qquad (2)$$

In the lab frame

$$\frac{dn_\gamma}{d\cos\Theta} = \frac{dn_\gamma}{d\cos\Theta'} \cdot \frac{d(\cos\Theta')}{d(\cos\Theta)} \quad .$$

From (2)

$$\frac{d(\cos\Theta')}{d(\cos\Theta)} = \frac{1 - \beta_\pi^2}{(1 - \beta_\pi \cos\Theta)^2}$$

and with (1) we arrive at

$$\frac{dn_\gamma}{d(\cos\Theta)} = 2\pi k \frac{1 - \beta_\pi^2}{(1 - \beta_\pi \cos\Theta)^2} \quad .$$

This is the distribution of γ-rays as a function of γ-ray angle with respect to the π^0 direction. Note that the angle of the pion with respect to the gamma ray direction Θ_π is just $-\Theta$. Since $\cos\Theta_\pi = \cos\Theta$ we have for a fixed gamma ray direction

$$\frac{dn_\gamma}{d(\cos\Theta_\pi)} = 2\pi k \frac{1 - \beta_\pi^2}{(1 - \beta_\pi \cos\Theta_\pi)^2} \frac{dN_\pi}{d\Omega_\pi}$$

where the final term is the distribution of the pion in the lab frame. For an isotropic distribution

$$\frac{dN_\pi}{d\Omega_\pi} = K$$

$$\frac{dn_\gamma}{d(\cos\Theta_\pi)} = 2\pi k K \frac{1 - \beta_\pi^2}{(1 - \beta_\pi \cos\Theta_\pi)^2} \qquad (3)$$

Now

$$\frac{dn_\gamma}{dE_\gamma} = \frac{dn_\gamma}{d(\cos\theta_\pi)} \frac{d\cos\theta_\pi}{dE_\gamma} = \frac{dn_\gamma}{d(\cos\theta_\pi)} \Big/ \frac{dE_\gamma}{d(\cos\theta_\pi)} \quad .$$

From appendix I.1

$$E_\gamma = \frac{1}{2} \frac{M_\pi^2}{E_\pi - P_\pi \cos\theta_\pi} \tag{4}$$

from which we derive

$$\frac{dE_\gamma}{d(\cos\theta_\pi)} = \frac{1}{2} \frac{P_\pi M_\pi^2}{(E_\pi - P_\pi \cos\theta_\pi)^2} \quad . \tag{5}$$

Combining (3) and (5) with the identity $(E_\pi - P_\pi \cos\theta_\pi) = E_\pi(1 - \beta\cos\theta_\pi)$ we obtain

$$\frac{dn_\gamma}{dE_\gamma} = \frac{4\pi k K (1 - \beta_\pi)^2 E_\pi^2}{P_\pi M_\pi^2} = \frac{4\pi k K}{P_\pi} \quad .$$

The total number of γ rays observed per unit energy interval is $\frac{dN_\gamma}{dE_\gamma}$ where

$$\frac{dN_\gamma}{dE_\gamma} = \int \frac{dn_\gamma}{dE_\gamma} \, d\Omega_\pi \quad ;$$

$$\frac{dN_\gamma}{dE_\gamma} = \frac{16\pi^2 k K}{P_\pi}$$

which is independent of the γ-ray energy. This formulation is valid as long as (4) is valid, i.e. for the energy range between E_L and E_H where

$$E_{H,L} = \frac{E_\pi \pm P_\pi}{2} \quad .$$

Clearly $\frac{dN_\gamma}{dE_\gamma} = 0$ outside of these limits. Hence for an isotropically distributed mono-energetic π^o we observe a γ-ray spectrum:

$$\frac{dN_\gamma}{dE_\gamma} = \begin{cases} 0 & E_\gamma < E_L = \frac{E_\pi - P_\pi}{2} \\ \frac{16\pi^2 kK}{P_\pi} & E_L < E_\gamma < E_H = \frac{E_\pi + P_\pi}{2} \\ 0 & E_\gamma > E_H \quad . \end{cases}$$

3. The Second-Gamma-Ray Cone Angle

The angle in the lab frame between the two γ-rays from the decay of a π^o with total energy E_π is completely determined by the energy E_π and the energy of one of the γ-rays E_1. The angle which we wish to find is ϕ, shown in figure AI.3.1.

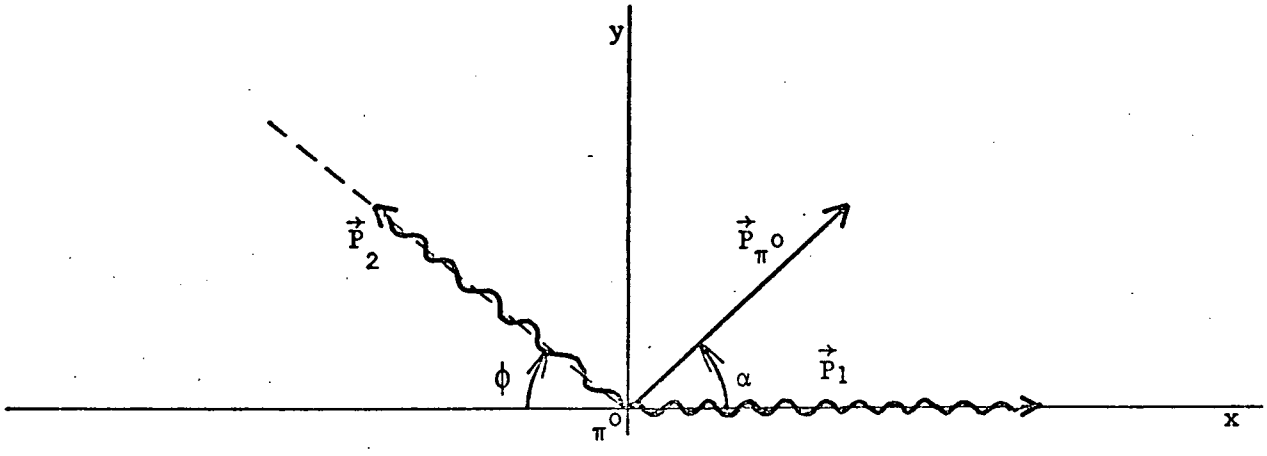

Figure AI.3.1 π^o Decay in the Lab Frame

The statements of conservation of energy and momentum are

$$P_1 = P_\pi \cos\alpha + P_2 \cos\phi \tag{1}$$

$$P_\pi \sin\alpha = P_2 \sin\phi \tag{2}$$

$$P_1 + P_2 = (M_\pi^2 + P_\pi^2)^{\frac{1}{2}} = E_\pi \tag{3}$$

From (2)

$$\cos\alpha = \pm \left(1 - \left(\frac{P_2}{P_\pi}\right)^2 \sin^2\phi\right)^{\frac{1}{2}} .$$

Using this (1) becomes

$$P_1 = \pm P_\pi \left(1 - \left(\frac{P_2}{P_\pi}\right)^2 \sin^2\phi\right)^{\frac{1}{2}} + P_2\cos\phi \quad .$$

$$P_1^2 + P_2^2\cos^2\phi - 2P_1P_2\cos\phi = P_\pi^2\left(1 - \left(\frac{P_2}{P_\pi}\right)^2 \sin^2\phi\right) .$$

$$P_1^2 + P_2^2 - 2P_1P_2\cos\phi = P_\pi^2 \quad .$$

Substituting from (3) for P_2 we get

$$P_1^2 + (E_\pi - P_1)^2 - 2P_1(E_\pi - P_1)\cos\phi = P_\pi^2 \quad .$$

$$\cos\phi = \frac{P_1^2 + (E_\pi - P_1)^2 - P_\pi^2}{2P_1(E_\pi - P_1)} \quad .$$

Since $E_1 = P_1$

$$\cos\phi = \frac{E_1^2 + (E_\pi - E_1)^2 - P_\pi^2}{2E_1(E_\pi - E_1)} = \frac{M_\pi^2}{2E_1(E_\pi - E_1)} - 1$$

or

$$\cos\frac{\phi}{2} = \frac{M_\pi}{2\sqrt{E_1(E_\pi - E_1)}} = \sin\frac{\psi}{2}$$

where ψ is the angle between the two γ-rays.

APPENDIX II

The Elementary Coincidence Efficiency

For a π^o of energy $(T_\pi, T_\pi + dT_\pi)$ the probability of observing a decay γ-ray of energy $(E_\gamma, E_\gamma + dE_\gamma)$ in collimator 1 solid angle $d\Omega_{c_1}$ is

$$dP_s(T_\pi) = 2 \frac{dN_\gamma}{dE_\gamma} dE_\gamma \frac{d\Omega_{c1}}{4\pi} \qquad \text{(AII.1)}$$

where $\frac{dN_\gamma}{dE_\gamma}$ is the normalized singles γ-ray box spectrum (appendix I.2) and the factor 2 is included to account for 2 γ-rays per π^o decay. The probability for a π^o to have energy $(T_\pi, T_\pi + dT_\pi)$ is

$$dP_\pi = \frac{dN_\pi}{dT_\pi} dT_\pi \qquad \text{(AII.2)}$$

where $\frac{dN_\pi}{dT_\pi}$ is the normalized π^o energy spectrum. For such a π^o decay it is shown in appendix I.3 that the second γ-ray lies on the surface of a cone of half-angle ϕ, given by

$$\cos\frac{\phi}{2} = \frac{M_\pi}{2\sqrt{E_\gamma(E_\pi - E_\gamma)}} \quad . \qquad \text{(AII.3)}$$

Furthermore, because the angular distribution of the π^o momentum is isotropic, the second γ-ray probability is uniformly distributed over the surface of the cone. Thus the probability for detecting the second γ-ray in spectrometer 2 is determined by the amount of this cone which intersects collimator 2. For the special case that the π^o decay occurs on the axis of collimator 2 this is just the intersection of two confocal circular cones (figure AII.1)

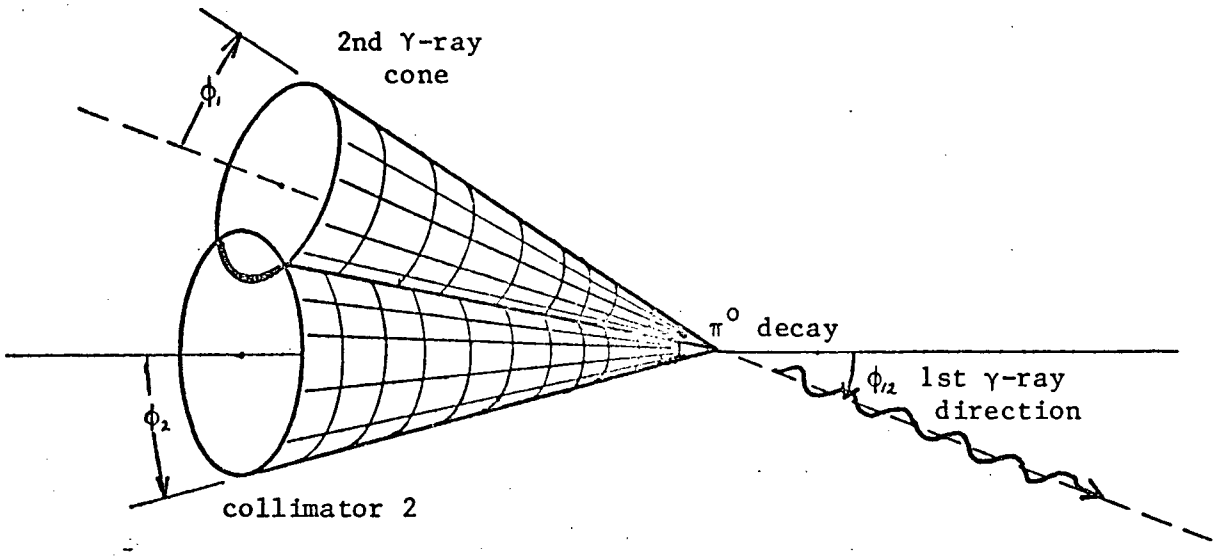

Figure AII.1 The Second γ-ray cone

ϕ_{12} is the angle between the first γ-ray and the collimator 2 axis, i.e. this is the angle between the axes of the collimator cone and the second γ-ray cone.

ϕ_1 is the half angle of the second γ-ray cone and is given by (AII.1)

ϕ_2 is the half angle of the collimator cone.

Consider the intersection of the two cones and the surface of a unit sphere with center 'o' at the focus of the cones (figure AII.2)

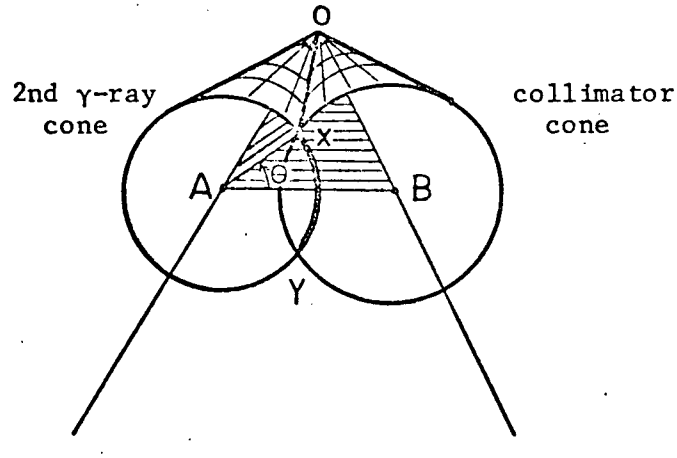

Figure AII.2 Intersection of two cones

The probability of detecting the second γ-ray is just $P_2 = 2\Theta/2\pi = \Theta/\pi$ where Θ is the angle between the OAX and OAB planes. If $\hat{e}_A$, $\hat{e}_B$, $\hat{e}_X$ are the unit vectors from the origin 'o' to the specified points then

$$\hat{n}_{OAB} = \frac{\hat{e}_A \times \hat{e}_B}{\sin\phi_1}$$

is the unit normal to the OAB plane and

$$\hat{n}_{OAX} = \frac{\hat{e}_A \times \hat{e}_X}{\sin\phi_1}$$

is the unit normal to the OAX plane. Then

$$\cos\Theta = \hat{n}_{OAB} \cdot \hat{n}_{OAX} = \frac{(\hat{e}_A \times \hat{e}_B) \cdot (\hat{e}_A \times \hat{e}_X)}{\sin\phi_{12}\sin\phi_1} .$$

The numerator may be expanded using standard vector identities to give

$$\cos\Theta = \frac{(\hat{e}_A \cdot \hat{e}_A)\ (\hat{e}_B \cdot \hat{e}_X) - (\hat{e}_A \cdot \hat{e}_X)\ (\hat{e}_B \cdot \hat{e}_A)}{\sin\phi_{12}\sin\phi_1} .$$

The dot products are easily evaluated and

$$\cos\Theta = \frac{\cos\phi_2 - \cos\phi_1\cos\phi_{12}}{\sin\phi_{12}\sin\phi_1} .$$

The probability for detecting the second γ-ray becomes

$$P_2 = \frac{\Theta}{\pi} = \frac{1}{\pi}\cos^{-1}\left(\frac{\cos\phi_2 - \cos\phi_1\cos\phi_2}{\sin\phi_{12}\sin\phi_1}\right) \qquad \text{(AII.3)}$$

and the probability of detecting a coincidence from a π^o of energy

$(T_\pi, T_\pi + dT_\pi)$ with one γ-ray energy $(E_\gamma, E_\gamma + dE_\gamma)$ in the element of solid angle $d\Omega_{c_1}$ in collimator 1 is just the product of (AII.1), (AII.2) and (AII.3);

$$dP_c = \frac{1}{2\pi^2} \cos^{-1}\left(\frac{\cos\phi_2 - \cos\phi_1\cos\phi_{12}}{\sin\phi_{12}\sin\phi_1}\right) \frac{dN_\gamma}{dE_\gamma} \frac{dN_\pi}{dT_\pi} d\Omega_{c_1} dE_\gamma dT_\pi \ .$$

APPENDIX III

The Deuterium Charge Exchange Phase Space

The rate for a transition from some initial state $|i\rangle$ to a final state $|f\rangle$ is given by

$$d\omega = \frac{2\pi}{h}|\langle f|H_{INT}|i\rangle|^2 d\rho$$

where $d\rho$ is the density of final states. For charge exchange in deuterium we have a three body final state (figure AIII.1) and in the center of mass frame

$$d\rho = d^3P_\pi d^3P_{n_1} d^3P_{n_2} \delta^3(\vec{P}_\pi + \vec{P}_{n_1} + \vec{P}_{n_2}) \delta(E_i - E_f)$$

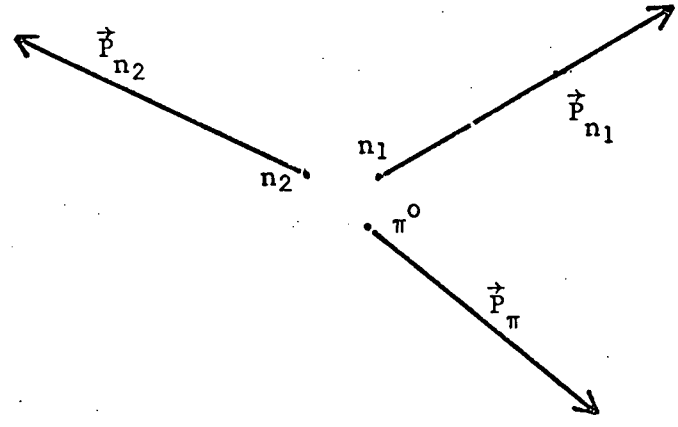

Figure AIII.1 - Deuterium Charge Exchange Final State

It is more convenient to use the set of vectors $(\vec{p},\vec{q},\vec{k})$ defined by

$$\vec{p} = \vec{P}_{\pi}$$

$$\vec{q} = \vec{P}_{n_1} - \vec{P}_{n_2}$$

$$\vec{k} = \vec{P}_{n_1} + \vec{P}_{n_2} \quad .$$

Then

$$d\rho = d^3\vec{p}\, d^3\vec{q}\, d^3\vec{k}\, \delta^3(\vec{p} + \vec{k})\, \delta(E_i - E_f) \quad .$$

The two neutrons are constrained to be in a relative p-state and the π^o - (nn) system must also be in a relative p-state. For small values of p and q the matrix element may be approximated as

$$< f|H_{INT}|i> = c|pq|$$

where c is just a constant of proportionality. The spectrum of the pions is just

$$\frac{d\omega}{dp} = c\int |pq|^2 d^3\vec{k}\, d^3\vec{q}\, p^2 d\Omega_p\, \delta^3(\vec{p} + \vec{k})\, \delta(E_i - E_f)$$

For small values of momentum the final energy is

$$E_f = \frac{p^2}{2m_{\pi}} + \frac{q^2}{4m_n} + \frac{k^2}{4m_n} \quad .$$

$$\frac{d\omega}{dp} = c\int p^4 q^2 d\Omega_p d^3\vec{q}\, \delta(E_i - \frac{p^2}{2m_{\pi}} - \frac{q^2}{4m_n} - \frac{p^2}{4m_n}) \quad .$$

$$\frac{d\omega}{dp} = c\int p^4 q^2 d\Omega_p d\Omega_q q^2 dq\, \delta(E_i - \frac{p^2}{2m_\pi} - \frac{q^2}{4m_n} - \frac{p^2}{4m_n}) \quad .$$

Now $\frac{dE_f}{dq} = \frac{q}{2m_n}$ so the final integration gives

$$\frac{d\omega}{dp} = 16\pi\, c(2m_n)p^4(4m_n(E_i - \frac{p^2}{2}\left(\frac{2m_n + m_\pi}{2m_n m_\pi}\right)))^{3/2} \quad .$$

With the identification of the reduced mass of the π^o-(nn) system as

$$\mu = \frac{2m_n m_\pi}{2m_n + m_\pi}$$

and noting that the maximum pion momentum is given by

$$\frac{P_{MAX}^2}{2\mu} = E_i$$

we see

$$\frac{d\omega}{dp} \sim p^4(p_{MAX}^2 - p^2)^{3/2} \quad .$$

Now

$$\frac{d\omega}{dE_\pi} = \frac{d\omega}{dp}\frac{dp}{dE_\pi} = \frac{d\omega}{dp}\frac{2m_\pi}{p} \quad .$$

Hence the energy spectrum of the pions is

$$\frac{d\omega}{dE} \sim p^3(p_{MAX}^2 - p^2)^{3/2}$$

or

$$\frac{d\omega}{dE_\pi} = CE_\pi^{3/2}(E_i - E_\pi)^{3/2}$$

where C is a normalization constant. The total rate is ω where

$$\omega = \int_{E_\pi=0}^{E_i} CE^{3/2}(E_i - E_\pi)^{3/2} dE_\pi \quad .$$

If we let $\eta = E_\pi/E_i$ the integral becomes

$$\omega = E_i^4 \, C \int_0^1 \eta^{3/2}(1 - \eta)^{3/2} d\eta \quad .$$

Hence $\omega \sim E_i^4$.

The initial energy E_i is the sum of the initial kinetic energy 'T' in the center of mass system and the Q value for the reaction. Thus

$$\omega \sim (T + Q)^4 \quad .$$

Now the cross section and rate are related by

$$\sigma \sim \frac{\omega}{v}$$

where v is the initial pion velocity. Then for low energies $v = (2T/m)^{\frac{1}{2}}$ and

$$\sigma = d \frac{(T + Q)^4}{\sqrt{T}}$$

where d is just a constant of proportionality.

Appendix IV

The Reduction of the Effective Hydrogen Contamination

In Section III.2 it was pointed out that there was a discrepancy in the effective concentration of hydrogen gas as determined from the number of hydrogen charge exchange events in the TINA singles spectrum and the hydrogen concentration in the gas phase determined from the quality of the deuterium oxide used to form the gas and a subsequent mass spectrometer measurement. These concentrations were

$$C_H \text{ (effective)} = 0.00145 \pm 0.00029$$

and

$$C_H \text{ (gas phase)} = 0.003 \pm 0.001$$

respectively. Thus the reduction in effective hydrogen concentration lies between 10% and 70%.

It is interesting to note that we are not alone in our observation of this phenomenon. The negative values of the charge exchange branching ratio, R, presented by all the previous authors (PA51, KL64, CH55) except Petrukin (PE64)[†] indicate an over estimation of the hydrogen background subtraction. A summary of these results was presented in Table I.1. Furthermore, in a recent report by Bisterlich et al (BI76) on the

[†]It should be mentioned here that Petrukin does not give enough detail of this measurement to definitely decide that they also have not measured a negative value for R.

reaction $\pi^- + {}^3H \rightarrow nnn\gamma$ in liquid tritium there is a clear indication of over-substraction of the hydrogen component of the γ-ray spectrum. In all these cases the hydrogen background has been subtracted by considering only the absolute hydrogen contamination in the gas phase.

There are two mechanisms which might contribute to this observed decrease in the effective hydrogen concentration. The first hypothesis is that simple distillation has taken place. The boiling point of liquid deuterium is about 3.2K higher than that of liquid hydrogen at atmospheric pressure and distillation may be used to separate these two isotopes (MC64). The action of this mechanism could be supported by the non-negative value of R reported by Petrukin and Prokoshkin(PE64) who have used a solid LiD target to make their measurement. This hypothesis is not well supported by the measurement of Panofsky et al (PA51) who have measured a negative value for R even with the use of a gas target, however the error of the measurement is so large that the distillation hypothesis could hardly be rejected on the basis of this measurement.

The second hypothesis is that we have observed the preferential absorption of pions into deuterium atomic states rather than hydrogen atomic states. The effect of preferential π^- capture on high Z nuclei in hydrogenous compounds is well known (KR68, P073, PE69). For a hydrogen-like atom the energy levels are given by (SH68)

$$E_n = - \frac{\mu Z^2 e^4}{2\hbar^2 n^2} \qquad \text{(A.IV.1)}$$

where the reduced mass, μ, which is slightly greater for the π^-d system

than for the $\pi^- p$ system, gives rise to bound states that are slightly deeper (≈6%) on the deuteron than on the proton.

Ponomarev (P073) has suggested the model of "Large Mesic Molecules" to account for the strong preference of the pion to be captured by the high Z fraction of hydrogenous compounds of the form $Z_m H_n$. The model presumes that the free pion is captured by the $Z_m H_n$ system by displacing one of the systems electrons. Since the only electron of the hydrogen atom is tied up in a molecular orbit the only possibilities are for the pion to be captured into either molecular orbits or isolated orbits of the Z atom. The probability for the former process is given by

$$W_1 = \frac{2n}{n + mZ}$$

Those pions captured into isolated atomic orbits of the Z atom ultimately undergo nuclear capture on the Z nucleus. Those pions captured into the common molecular orbits undergo transition to either the isolated Z atomic orbits or isolated hydrogen atomic orbits. The probability for the latter process is W_2 where

$$W_2 = 1/Z^2 \ .$$

The π^- systems which are thus formed move through the surrounding matter and undergo collisions with other nuclei. During these collisions the probability of transfer of the pion to a Z nucleus is proportional to the concentration of these nuclei.

$$\omega_T = \alpha n_Z$$

where n_Z is the number of Z nuclei per unit volume and α is a constant of proportionality. The de-excitation of the π-p system and subsequent nuclear capture by the proton are also enhanced by these collisions and the rate for these processes is thought to be proportional to the concentration of hydrogen nuclei.

$$\omega_c = \beta n_H$$

where n_H is the number of hydrogen nuclei per unit volume and β is a constant of proportionality. The probability for the meson to be captured by the hydrogen nucleus then is

$$W_3 = \frac{\beta n_H}{\beta n_H + \alpha n_Z} = (1 + \lambda C)^{-1}$$

where $C = n_Z/n_H$ and $\lambda = \alpha/\beta$. In the case of most hydrides the constant λ is believed to be small and hence it is thought that atomic transfer of the pion will not contribute greatly to the overall probability of pion capture on the hydrogen nucleus. This probability then is

$$W = W_1 W_2 = anZ^{-2}/(n + mZ) \qquad \text{(A.IV.2)}$$

which gives a good fit to the data of Krumshtein et al (KR68) with the constant $a \simeq 1.28$.

We see from equation A.IV.1 that we could construct a gedanken

nucleus, $D^{\prime}$, to replace the deuterium nucleus where the mass would be the same as the hydrogen mass but the value of Z would be

$$Z = 1.034.$$

Such a nucleus would have the same π^- atomic structure as the real deuterium nucleus. Unfortunately one can not apply equation A.IV.2 directly to such a nucleus. First of all for this $H\text{-}D^{\prime}$ system the arguments used to determine W_1 would not apply. In this case in fact only molecular orbits would be expected to occur since both available electrons are consumed in molecular orbits. Thus

$$W_1 \simeq 1.$$

Further, the argument that W_3 plays no role is based on the smallness of λC. In the present case the concentration is very large, $C = n_Z/n_H = 332$ and comments by Ponomarev (P073) indicate that $\lambda = kZ$ where k could be of the order of 0.3. Thus

$$W_3 \simeq (1 + kCZ)^{-1}$$

and even the small value of Z will be significant. In this case

$$W = W_1W_2W_3 = a/Z^2\ (1 + kCZ).$$

The constant of proportionality may be determined by noting that as

$Z \to 1$ the probability, W, must be determined by the concentration of hydrogen. That is

$$W(Z = 1) = \frac{n_H}{n_H + n_Z} = \frac{1}{1 + C} .$$

In the present case a = 0.3 and with Z = 1.034 we find that the probability for nuclear capture on hydrogen (i.e. the "effective hydrogen concentration") is

$$W = 0.00269 ,$$

or about a 10% reduction from the actual concentration. Whereas this result is in keeping with the range of our observed reduction it would be premature to state that this is the mechanism which we have observed. The errors in our measurement of the effect are very large and the possibility of distillation is by no means excluded. It will be necessary to make careful measurements of the effect using a gas target so distillation effects may be eliminated before any firm statement can be made. Such a study is being planned for the near future (ME77).